Chem Soc Rev

REVIEW ARTICLE

View Article Online
View Journal

MOF-based electronic and opto-electronic devices

Cite this: DOI: 10.1039/c4cs00096j

V. Stavila, A. A. Talin and M. D. Allendorf*

Metal–organic frameworks (MOFs) are a class of hybrid materials with unique optical and electronic properties arising from rational self-assembly of the organic linkers and metal ions/clusters, yielding myriads of possible structural motifs. The combination of order and chemical tunability, coupled with good environmental stability of MOFs, are prompting many research groups to explore the possibility of incorporating these materials as active components in devices such as solar cells, photodetectors, radiation detectors, and chemical sensors. Although this field is only in its incipiency, many new fundamental insights relevant to integrating MOFs with such devices have already been gained. In this review, we focus our attention on the basic requirements and structural elements needed to fabricate MOF-based devices and summarize the current state of MOF research in the area of electronic, opto-electronic and sensor devices. We summarize various approaches to designing active MOFs, creation of hybrid material systems combining MOFs with other materials, and assembly and integration of MOFs with device hardware. Critical directions of future research are identified, with emphasis on achieving the desired MOF functionality in a device and establishing the structure–property relationships to identify and rationalize the factors that impact device performance.

Received 2nd March 2014

DOI: 10.1039/c4cs00096j

www.rsc.org/csr

Introduction

During the past decade metal–organic frameworks (MOFs) have emerged as a promising class of materials with a wide spectrum of useful applications.[1–3] MOFs are hybrid materials, having both an inorganic and an organic component. Their structure is comprised of metal ions or clusters that are connected by electron-donating "linker" groups to create a networked structure with well-defined pores. The tunable pore size of MOFs, which ranges from <1 nm to ~ 10 nm,[4] makes them extremely versatile for applications that involve host–guest interactions.[5]

Sandia National Laboratories, P.O. Box 969, Livermore, California 94551-0969, USA. E-mail: mdallen@sandia.gov

V. Stavila

Vitalie Stavila received his doctorate in Inorganic Chemistry from the State University of Moldova in 2002. He carried out postdoctoral work at Ecole Normale Supérieure de Lyon (France) and at Rice University in Houston, Texas (USA). Dr Stavila is currently a Senior Member of Technical Staff at Sandia National Laboratories in Livermore, California (USA), where his research focuses on experimental aspects of materials science geared toward energy storage and nanoscale fabrication. His research interests include the development of metal–organic frameworks that can act as active materials in photodetectors, chemical sensors and solar cells.

A. A. Talin

A. Alec Talin is a Principal Member of Technical Staff at Sandia National Laboratories, in Livermore, CA, an adjunct fellow at the Center for Nanoscale Science and Technology at NIST, Gaithersburg, MD, and an adjunct associate professor of Materials Science and Engineering at the University of Maryland, College Park. He received a BA in Chemistry from UC San Diego in 1989 and a PhD in Materials Science and Engineering from UC Los Angeles in 1995. His interests include novel electronic materials and devices, charge transport at contacts and interfaces, and electrochemical energy conversion and storage.

These advantages are compelling and, as a result of their susceptibility to rational design,[6,7] both superior properties compared with conventional nanoporous materials and new understanding with respect to the interaction of small molecules confined within pores are being achieved. Not only do MOFs allow for enhanced uptake of various species (in part due to their large pore volumes and surface areas), they can also exclude certain molecules based on their size, shape, polarity, and conformation. This selectivity makes MOFs promising active materials for gas sorption,[1,2,5,8] separation materials and devices such as membranes and preconcentrators,[9,10] and chemical sensors,[11] applications that have traditionally used porous materials that are either crystalline, but fully inorganic (*e.g.*, zeolites), or fully organic, but disordered (*e.g.* aerogels or organic polymers). MOFs marry the intrinsic value of each, providing both a high degree of synthetic versatility and an ordered structure that enables rational design.

It is not difficult to envision using MOFs for photonic and electronic devices and energy storage, but these topics have received far less attention than the typical applications of nanoporous materials listed above.[12] Their advantages for these purposes are numerous. First, MOFs have an ordered structure determined (largely) by the coordination geometry of the metal and the topology of the linkers. The strong chemical bonds created by this self assembly process enable rational design,[13] a process that has been termed "reticular synthesis,"[7] as well as providing high thermal and chemical stability. Thus, MOF pore dimensions are highly defined compared with conventional amorphous nanoporous materials and polymers. Not only is this sub-angstrom knowledge of atomic positions advantageous for determining fundamental structure–property relationships, it eliminates the disorder that is a major contributor to poor mobility and low carrier densities in organic conductors, relative to crystalline inorganic materials such as silicon. Second, MOFs possess a high degree of synthetic flexibility that allows their intrinsic electrical, optical, and mechanical properties to be tuned.[10] This has lead to a remarkable range of electronic, photonic, and magnetic behaviors: ferroelectric,[14,15] ferromagnetic,[16,17] antiferromagnetic,[18,19] low-κ dielectrics,[20–22] proton-[23,24] and ion-conducting,[25,26] luminescent,[27–29] and non-linear optical properties[30,31] have been described. Although the vast majority MOFs are insulators,[32] a few semiconducting frameworks are known and theoretical predictions suggest many more are possible.[33] Moreover, their porosity provides opportunities to introduce non-native functionality by infusing the accessible volume with guest molecules; for example, electrical conductivity has been achieved in the MOF HKUST-1 by introducing redox-active molecules into the pores.[34] Finally, mild processing routes are now available that are compatible with most substrates. Consequently, MOFs (see Fig. 1 for representative structures) possess many of the properties of an "ideal material" with uses in batteries, fuel cells, displays, sensors, LEDs, photodetectors, scintillators, lasers, and radio-frequency identification (RFID) tags, to name just a few. The limited examples of conducting and semiconducting MOFs suggests intriguing possibilities as interconnects, field-effect transistors (FETs), thermoelectrics, and piezoresistors as well. In these examples, the MOF would play an active role in generating, transporting, or storing energy or charge, leading us to coin the name "MOFtronics" to describe this emerging field.

The objectives of this article are to review recent literature describing the properties of MOFs relevant to their use in electronic devices and to assess the current status of the research concerning their integration with other materials to create devices with novel capabilities. Here, "device" is defined rather broadly to include sensors, transistors (*i.e.*, logic), photovoltaics, and photocatalysts. We first review the basic requirements and structural elements required to fabricate MOF-based devices, including the critical technology needed to grow MOF thin films. Progress toward developing electrically conducting frameworks is then surveyed, where several recent discoveries should encourage further research. Subsequent sections discuss examples of incorporating MOFs as active components of light harvesting and chemical sensing devices. Finally, we identify critical challenges impeding the incorporation of MOFs into functional devices.

M. D. Allendorf

Mark Allendorf is a Senior Scientist at Sandia National Laboratories in Livermore, CA. He is President Emeritus and Fellow of the Electrochemical Society. Dr Allendorf received his PhD in inorganic chemistry from Stanford University. His research includes Metal–Organic Frameworks (MOFs) for a variety of electronic device applications, including chemical sensors and photovoltaics, and the creation of emergent properties by using MOFs as templates and hosts for molecules and molecular or atomic clusters. In addition, he has worked extensively in the high-temperature chemistry of solar fuel generation, chemical vapor deposition, and catalytic combustion.

Integration of MOFs with functional devices

Incorporating MOFs into device hardware requires a direct physical interface with another material. To accomplish this, MOFs are typically grown as films or deposited as coatings on various substrates. Selected applications, such as photovoltaics, membranes, and sensors require strict control over the quantity and quality of the MOF film or coating. In many cases, the film processing method is specific to the desired MOF. However, several general growth methods have been developed in the last few years; several excellent review articles on this topic are available.[35–37] In this section, we focus on the latest advances in the growth of MOF films, with a particular focus on the general synthetic approaches applicable to MOF integration with devices.

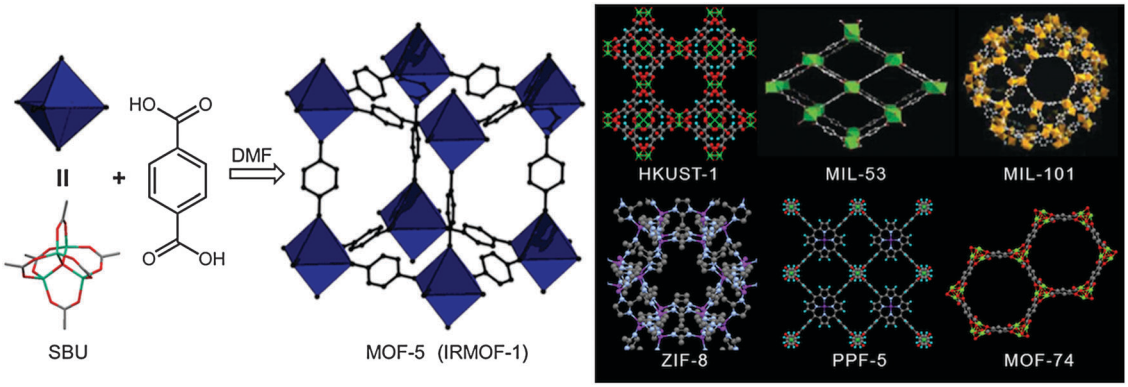

Fig. 1 Left: schematic representation of the SBU assembly in MOF-5; right: representative MOF structures for device applications.

One of the first steps in systematic fabrication of MOF-based devices involves deposition of a MOF film or coating on a substrate. The deposition of MOF thin films can be achieved using *in situ* and *ex situ* methods.[12] *In situ* methods rely on substrate functionalization to allow preferential nucleation of MOF molecules and subsequent film growth, while *ex situ* methods are based on direct deposition of previously synthesized MOF crystals on surfaces. An extremely versatile layer-by-layer MOF growth deposition technique was discovered by Fischer, Wöll and co-workers[38,39] and involves the sequential reaction of the metal precursor with the organic linker, both of which are in solution. During immersion, the metal ions bind to the upper layers of ligands and *vice versa*, allowing the building of the SURMOF (SURface-mounted Metal–Organic Frameworks) structure. *In situ* surface plasmon resonance (SPR) studies[40] indicate a linear growth mechanism, with the MOF film thickness directly proportional to the number of immersion cycles. Another remarkable feature is that the nature of the terminating groups of the self-assembled monolayers (SAMs) (COOH or OH) governs the crystal growth direction ({100} or {111}), with the surface COOH groups coordinating to the Cu_2 paddlewheel, while the OH groups are presumably involved in strong hydrogen bonding with the H_2O molecules in the apical position of the Cu(II) paddle-wheel center. We recently applied the Quartz Crystal Microbalance (QCM) technique to observe the kinetics of step-by-step growth of HKUST-1 on various substrates, and based on the measured reaction rates proposed a possible mechanism.[41] The results indicate that the step-by-step deposition of HKUST-1 on surfaces (Fig. 2) is initiated by deposition of Cu(II) on the surface, followed by ligand exchange between coordinated acetate from the copper precursor and benzene-1,3,5-tricarboxylate ligands, leading to crystallite coalescence to form a dense film.[40–42] This process has two key advantages. First, the self-limiting growth, akin to atomic layer deposition (ALD), should allow conformal growth on small and high aspect-ratio features. Second, each complete cycle of the LbL process allows the thickness to increase by only one structural unit (*i.e.* combination of metal ion and linker), yielding precise control over layer thickness.

MOF films have been deposited on a wide variety of substrates with different composition, roughness and porosity, including metals, oxides, polymers, graphene, textiles, *etc.*[12,35,37] In most cases the choice of substrate is determined by the intended application. For example, a transparent conducting oxide is needed for photovoltaic applications, a semiconducting layer, such as TiO_2 or ZnO, is needed for dye-sensitized solar cells (DSSC), and a metal or metal oxide is required for surface acoustic wave (SAW) sensors. Gold was one of the first substrates used to grow MOF films because its surface functionality can be controlled by the formation of SAMs. Terminal groups of SAMs attached to gold can be selected to bind metal ions (COOH, OH, and pyridine groups are typical) and display low surface roughness. One of the main problems in using SAMs is their poor thermal

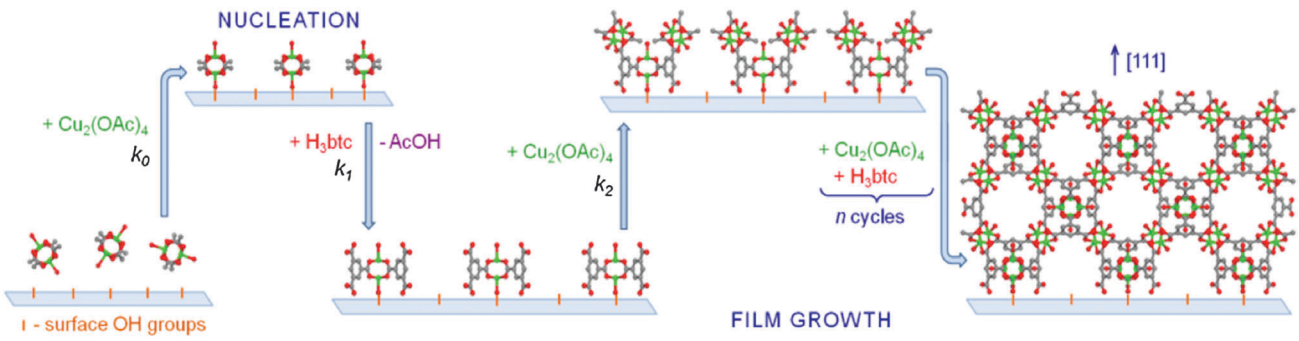

Fig. 2 Schematic representation of the proposed model for $Cu_3(btc)_2$ nucleation and growth on oxide surfaces. The atoms are shown as follows: Cu – green, O – red, C – gray. Reproduced with permission from ref. 41.

and chemical stability. Another potential issue with SAMs of alkyl thiols for achieving low resistance electrical contact is their insulating nature. Oxide substrates (silica, alumina, titania) are of interest because they are cheap and temperature- and corrosion-resistant, making them ideal for device applications. One disadvantage of oxides is lack of control over the surface composition. Although OH groups are typically found on native oxide surfaces, their density varies and is difficult to control. Oxygen plasma or chemical treatment (with NaOH, KOH, *etc.*) steps can be beneficial to fully hydroxylate the oxide surface in order to promote uniform MOF film nucleation and growth.

Thin film growth of HKUST-1 has been studied extensively and, more recently, several other paddlewheel-type MOFs have been deposited as thin films on various surfaces. H. Kitagawa and co-workers used the step-by-step growth technique to fabricate thin films of $[Fe(pz)][Pt(CN)_4]$.[43] Other examples include IRMOF-1 (originally known as MOF-5) films reported by Mertens *et al.*,[44] and $[Zn_4O(dmcapz)_3]$ (dmcapz = 3,5-dimethyl-4-carboxypyrazolato).[45] Another strategy has been employed by H. Kitagawa's group, which introduced a versatile technique to grow MOF layers *via* Langmuir–Blodgett techniques.[46,47] The individual MOF layers are transferred onto a silicon substrate, with intermediate washing steps between the assembly cycles. Thin films of porphyryn-based NAFS-1 and NAFS-2 MOFs can be isolated as highly oriented thin films and represent the first examples of MOFs isolated as SURMOFs on surfaces, but not in bulk.

R. Fischer *et al.* further advanced the LbL concept by assembling MOF thin films incorporating distinct functionalities in the same framework by using multiple metal ions or linkers of the same or different topology. This concept offers a new dimension for controlling pore size, pore opening, distribution of chemical function, and overall composition, allowing MOF properties to be tailored beyond the limits of mono-functional MOFs. For example, films of heterometallic isostructural MOFs have been described, as in the case of $[Cu_2(ndc)_2(dabco)]/[Zn_2(ndc)_2(dabco)]_n$.[48] In another example, films of $[Zn_4O(bdc\text{-}NO_2)_{0.74}\{bdc\text{-}(OAl)_2\}_{1.06}\{bdc\text{-}(OBz)_2\}_{1.20}]$ were found to display a higher selectivity for adsorbing CO_2 over CO than the parent IRMOF-1 structure.[49] Functional groups on the surface (*e.g.*, terminal components of self-assembled monolayers) may nucleate MOF growth in a specific crystallographic direction, leading to preferentially oriented films.[36,50]

The concept of selecting anchoring groups of a MOF on a surface was first demonstrated for IRMOF-1 using a patterned $COOH/CF_3$-terminated SAMs.[51] IRMOF-1 cannot grow on a CF_3-terminated SAM, but only on COOH-groups, allowing the formation of a 500 nm-thick non-oriented films made of 100 nm cubic crystallites after 24 h. The concentrated solution has to be pre-treated solvothermally to initiate the formation of the SBUs; the deposition of the film is then continued at room temperature upon slow crystallization conditions. Subsequent studies showed that selective nucleation of IRMOF-1 can also occur on carboxylic acid-terminated SAMs on SiO_2 and ultrathin, amorphous Al_2O_3 adhesion layers, demonstrating the possibility to obtain patterned MOF thin films on a variety of substrates.[52] Similar growth conditions also proved successful for MIL-88B (Fe) film formation[53] and a series of pillared MOFs.[37,54] Although quite interesting in terms of the properties displayed, this first generation of MOF thin films displayed only a single functionality.

A significant development recently reported by R. Fischer's group is the isolation of the first *multivariate* (multiple functionality) layered MOF thin films[55] The parent MOF, $[Cu_2(ndc)_2(dabco)]$, crystallizes in the tetragonal system containing two surfaces terminated by copper–ndc (denoted as [001] planes) and four surfaces terminated by copper–dabco (denoted as [100] planes) (Fig. 3). Based on the different possible orientations of the ndc linkers in the framework, the pore openings in [001] and [100] directions were evaluated to range from 7×2 Å^2 to 7×5.7 Å^2 and 2×2 Å^2 to 5.7×5.7 Å^2, respectively. $[Cu_2(ndc)_2(dabco)]$ oriented in [001] and [100] direction (denoted as $SURMOF_{001}$ and $SURMOF_{100}$) were fabricated on pyridyl- and carboxylate-terminated self-assembled monolayers (SAMs) on gold-coated quartz crystal microbalance (QCM).[55] Based on the orientation of the films, both the kinetics and thermodynamics of gas adsorption can be systematically tuned, which makes this approach promising for the design of highly selective gas separation membranes.

Alternating layers of ZIF-8 and mesoporous TiO_2 were fabricated by Lotsch and Bein to form uniform Bragg stacks heterostructures.[57] The resulting photonic device is composed of multilayers of the two components with different refractive indices. ZIF-8 was selected to impart molecular selectivity, while the role of mesoporous TiO_2 was to enable a sufficient contrast in the refractive index within the Bragg stack. Alcohols with various lengths of the alkyl chain were shown to display differentiating sorption behavior on the as-assembled Bragg stack. These results indicate possible applications of multilayered MOF-based heterostructures in optical sensors.

Although development is at a very early stage, the heteroepitaxial growth of MOF thin films represents a new step toward

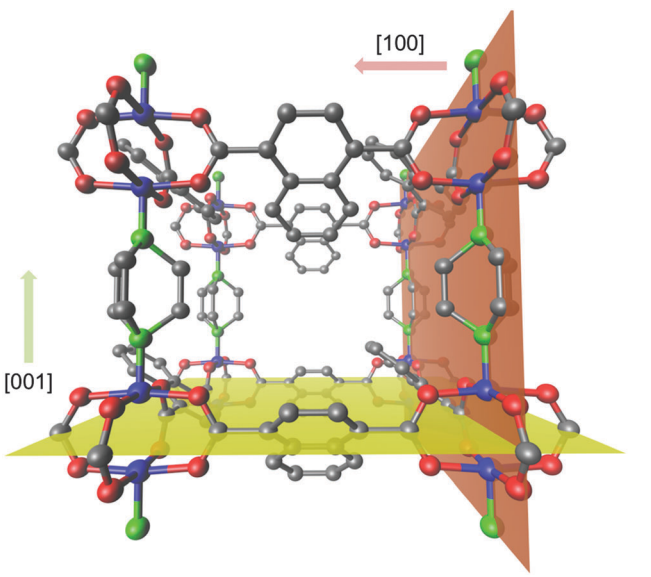

Fig. 3 Tetragonal $[Cu_2(ndc)_2(dabco)]$ films oriented in [001] and [100] direction fabricated on pyridyl- and carboxylate-terminated self-assembled monolayers (SAMs). Adapted from ref. 56.

expanding the range of possible functionalities that can be incorporated into a MOF film. MOFs offer unique possibilities for modifying isostructural networks; for instance, the IRMOF series comprises various sized linkers sharing the same topology.[58] Single-crystals of a $[Cu_2(ndc)_2(dabco)]$ shell around a $[Zn_2(ndc)_2(dabco)]$ core[59] and (IRMOF-1)@(IRMOF-3)@IRMOF-1 and (IRMOF-3)@(IRMOF-1)@IRMOF-3 Matryoshka crystals[60] were also reported.

A heteroepitaxial hybrid film IRMOF-1@IRMOF-3 was synthesized solvothermally by depositing IRMOF-3 on a seeding layer of IRMOF-1 (MOF-5).[61] The step-by-step approach was used to fabricate high quality heterostructured MOFs based on the concept of lattice matched building blocks.[13,56,62] Very recently, Tu and Fischer fabricated a thin film heterostructure from two SURMOFs of different topology: $Cu_3(btc)_2$ on top of $Cu_2(ndc)_2(dabco)$.[63] The heterostructured MOF bilayer was deposited on QCM electrodes using a step-by-step approach, resulting in selective uptake adsorption properties for methanol, 1,3,5-trimethylbenzene and 1,3,5-triisopropylbenzene. Deposition methods which rely on sequential immersion of the substrate in a solution are particularly well-suited for fabrication of heterostructured MOFs as one of the building units (metal, linker) can easily be replaced as some point in the synthesis. Other multifunctional MOFs have been reported; however, their deposition as thin films on surfaces has not been demonstrated so far.[49,64,65]

Electronically conductive MOFs

The salient feature of polymers and organic molecular solids that conduct electricity is the presence of delocalized π-bonding networks that facilitate the flow of mobile charges. In a manner analogous to inorganic semiconductors, dispersion in valence and conduction bands can emerge in organic materials provided there is sufficient wave function coupling along conjugated 1D-polymer chains or along π-stacked conjugated molecules.[66] However, even in highly aromatic polymers and molecular solids the bandwidth may be considerably narrower compared to their inorganic counterparts due to lower atomic density. The narrower bandwidth, or limited curvature of the electronic bands, results in higher effective masses for electrons and holes, leading to small polaron formation and carrier localization. Carrier localization is further enhanced in organic materials by structural disorder, reduced dielectric screening, and strong electron–phonon coupling, resulting in thermally activated hopping as the dominant transport mechanisms in many organic semiconductors rather than true band transport.[67] To date, the highest mobility observed in polymers with relatively long-range order, such polythiophene derivatives incorporating fused thiophene rings, is $\sim 1\ cm^2\ V^{-1}\ s^{-1}$, orders of magnitude below the values typically observed for crystalline inorganic semiconductors.[68]

Whereas interest in electrically conducting porous MOFs has only recently emerged, crystalline hybrid (organic–inorganic) coordination polymers (HCPs) with metallic, semi-conducting, insulating, and resistance switching characteristics have been extensively studied over the past several decades.[69] HCPs provide within a single material the highly ordered structure of inorganic conductors with the chemically tailorable properties and low cost of organics. As in the case of all-organic conductors, charge mobility in HCPs requires an extended bonding structure that supports delocalized electrons. This is achieved by coupling between the ligand π and metal d orbitals. An early example of a HCP extensively investigated for its optical, magnetic and, more recently, electrical properties is Prussian blue (PB). PB crystallizes in a simple cubic structure with cyanide ligands coordinated to alternating Fe^{2+} (low spin) and Fe^{3+} (high spin) ions as shown in Fig. 4. The blue color arises from a broad absorption band at ~750 nm assigned to a metal-to-metal charge transfer transition from C-coordinated Fe^{2+} ions across the CN ligand to N-coordinated Fe^{3+} ions.[70,71] The charge transfer process in HCPs is often described using the donor–bridge–acceptor terminology originally developed in the context of electron transfer in mixed-valence molecules such as $[(NH_3)_5Ru^{2+}(4,4'\text{-bipyridine})Ru^{3+}(NH_3)_5]^{5+}$.[72] Following the work of Robin and Day, the magnitude of the electronic coupling of the donor and acceptor sites, expressed as the electron coupling matrix element H_{AB}, can be used to distinguish donor–bridge–acceptor systems into classes. In class I systems the coupling is very weak, (*i.e.* $H_{AB} \sim 0$) and the donor and acceptor behave like separate sites; the energy barrier (or activation energy) for charge transfer, $\Delta G^* = (\lambda - 2H_{AB})^2/4\lambda$, where λ is the reorganization energy, corresponds to the intersection of the dashed red curves shown in Fig. 4.

For class II systems ($0 < H_{AB} < \lambda/2$) the degree of charge transfer is intermediate: there are new optical absorption bands

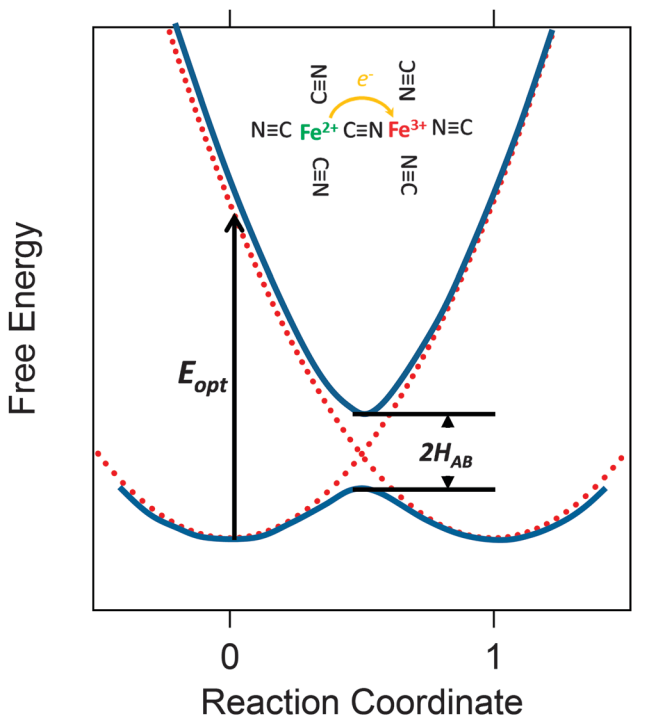

Fig. 4 Free energy *vs.* reaction coordinate for the initial and final diabatic states (dashed red parabolas) and the lower and upper adiabatic states (blue curves) of a symmetric ($\Delta G = 0$) mixed-valence system. E_{opt} is the energy of the donor–acceptor (metal-to-metal or intervalence) charge transfer transition and H_{AB} is the electronic coupling matrix element between the two diabatic states (adapted from ref. 72).

indicative of charge transfer, but the ground state maintains a double-well potential, indicating substantial localization. For class III systems, $H_{AB} \geq \lambda/2$ and $\Delta G^{*} = 0$, indicating complete charge delocalization. PB is a class II compound with $0 < H_{AB} < \lambda/2$ implying an intermediate level of electron delocalization. As synthesized, PB is an insulator, but can be turned into an ohmic conductor by either oxidation to form Berlin green, which introduces positively charged holes (balanced by intercalation of counter ions such as Cl^{-} to maintain charge neutrality), or reduction to form Prussian white (counter balanced by K^{+}, for example). Conduction in oxidized or reduced PB, however, is by thermally activated hopping with activation energy of $\sim$0.030 eV.[73] The hopping mechanism with low activation energy is consistent with the type II Robin Day classification, which implies only partial electron delocalization. In contrast, in metals or crystalline semiconductors with fully ionized dopant impurities the conductivity *decreases* with increasing temperature due to scattering with phonons. Hopping conduction can also be rationalized based on the relatively large separation of Fe ions in PB (unit cell is $\sim$10.2 Å) which leads to lower orbital overlap and flatter bands, as well as the compound's low dielectric constant, which decreases dielectric screening and therefore increases charge localization.[74]

A variety of electrically conducting HCPs, consisting of transition metals bonded to organocyanide ligands such as tetracyanoquinodimethane (TCNQ), tetracyanoethylene (TCNE), and dicyanoquinonediimine (DCNQI), have been identified.[75] For example, TCNQ forms 2-dimensional fishnet structures with a paddlewheel diruthenium complex, $[Ru_2II,II(O_2CCF_3)_4]$.[76] The degree of metal-to-ligand charge transfer in this system can be affected by substituting TCNQ with its (partially) brominated, chlorinated or fluorinated analogues. Only in the case of F_4-TCNQ is there full transfer of charge as evidenced by magnetic susceptibility and vibrational spectroscopic measurements. The electrical conductivity for these non-porous MOFs increases from $\sim 10^{-7}$ S cm^{-1} for unsubstituted TCNQ to $\sim 10^{-5}$ S cm^{-1} for F_4-TCNQ, and exhibits hopping characteristics with activation energy of $\sim$0.3 eV. With interlayer distance of 6.6 Å, there is little π–π overlap between the 2D sheets, and conduction primarily occurs within the layers. Electrical conductivity has also been extensively studied in various TCNQ-based charge transfer complexes with Cu, Ag, alkali metals, as well as organic molecules such as tetrathiafulvalene (TTF), all of which assemble into columnar stacks of $A^{+}D^{-}$ with TCNQ interplanar distances of $\sim$3.5 Å.[77–79] Conduction in these materials is through the π-stacked TCNQ molecules, rather than through the metal–ligand bond, and values $>10^{3}$ S cm^{-1} at room temperature have been reported.[78,79]

Guided by the knowledge gained from the extensive studies of conducting organic and coordination polymers, a number of groups recently demonstrated promising strategies for realizing conducting MOFs with permanent porosity. The first porous conducting MOF was reported by Kobayashi *et al.* and consisted of nickel bis-dithiolate complexes connected by square planar Cu(pyrazine)$_4$ units, forming a framework with narrow one-dimensional channels.[80] Although the conductivity of the as-prepared Cu[Ni(pdt)$_2$] (pdt^{2-} = pyrizine 2,3-dithiolate) MOF was low, $\sim 10^{-8}$ S cm^{-1}, it increased to $\sim 10^{-4}$ S cm^{-1} after partial oxidation of the framework with I_2 vapor. Reaction of the framework with I_2 introduces positively charged holes into the framework *via* the $[Ni(pdt)_2]^{2-/1-}$ complex reversible redox couple at $E_{1/2} = -0.391$ V (*vs.* Ag/AgCl). However, charge transport is still thermally activated, with an activation energy of $\sim$0.200 eV. Since the conductivity measurements were carried out on polycrystalline films with uncharacterized defect structure, it is difficult to state whether the origin of hopping conduction is due to narrow bandwidth and poor screening (as is the case for PB) or to a high concentration of electrically active traps.

In 2012, Gandara *et al.* described an Fe-triazolate MOF that crystallizes with a cubic $Fd\bar{3}m$ structure and a pore diameter of 4 Å; this material exhibits thermally activated transport with conductivity of $\sim 10^{-3}$ S cm^{-1}. As in the case of the Cu[Ni(pdt)$_2$] framework, oxidizing the Fe triazolate MOF with I_2 increased the conductivity to $\sim 10^{-2}$ S cm^{-1} by forming excess holes localized on the Fe ions. Although intriguing, these frameworks provide limited flexibility for expanding the suite of conducting frameworks. The Fe-triazolate MOF is one of an isoreticular series in which other metal ions are used, none of which is conducting. Alternatively, expansion of the pores to accommodate species other than very small molecules is limited to two dimensions by the topology of the pdt linker.

As an alternative to the 'through bond' strategy for achieving charge delocalization, Narayan *et al.* recently reported a conducting porous framework, Zn_2(TTFTB), (TTFTB = tetrathiafulvalene tetrabenzoate) consisting of columnar π-stacks of TTFTB linkers coordinated to Zn^{2+} ions *via* the carboxylate groups.[81] The effectiveness of π-stacking electroactive molecules like porphyrins, phthalocyanins, and triphenylenes for enabling charge transport in porous materials has already been demonstrated in a number of COFs, and is therefore a promising strategy for assembling conducting MOFs.[82,83] Zn_2(TTFTB) adopts a helical structure with TTF molecules aligning approximately perpendicular to the screw axis along the center and $\sim$3.8 Å apart, surrounded by a backbone of hexagonally arranged Zn-carboxylates and 1D pores $\sim$6 Å in diameter (Fig. 5). Flash photolysis-time-resolved microwave conductivity (FP-TRMC) was used to measure a charge mobility of $\sim$0.2 cm^2 V^{-1} s^{-1}. Unlike field-effect transistor (FET) and Hall techniques, FP-TRMC measures mobility over few nanometers length scale, thus providing the intrinsic value for a given material, not bounded by carrier scattering at grain boundaries and charged interfaces.[67] The same group also very recently demonstrated a conducting porous MOF using the linker 2,5 disulfhydrylbenzene-1,4-dicarboxylic acid (H_4DSBDC) and Mn metal to generate Mn_2(DSBDC).[84] This MOF is structurally similar to a class of frameworks containing infinite 1D SBUs in which single oxygen atoms bridge pairs of metal ions with the general formula M_2(DOBDC) M = Mg, Mn, Fe, Co, Ni, Zn; DOBDC = dihydroxybenzene-1,4-dicarboxylic acid).[6] In Mn_2(DSBDC) one Mn^{2+} ion is coordinated by four carboxylate oxygen atoms and two thiophenoxide groups, while another Mn^{2+} ion is coordinated by two carboxylate oxygen atoms, two thiophenoxide groups and two *cis*-oriented DMF solvent

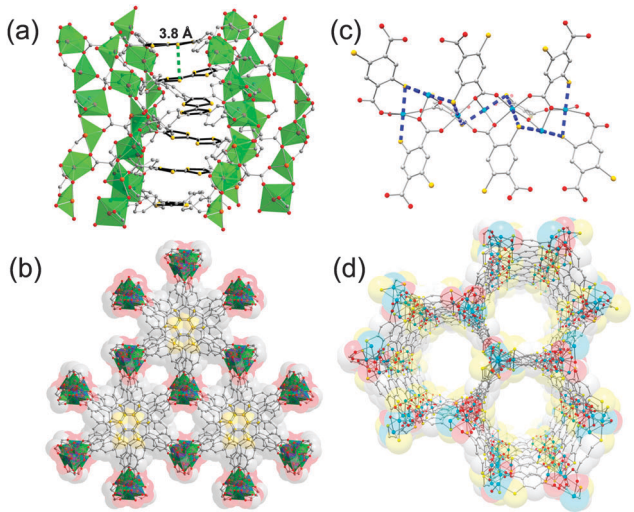

Fig. 5 (a) Side view of a helical TTF π-stack in Zn_2(TTFTB) indicating the shortest intermolecular S···S distance; (b) a view of the benzoate-lined infinite pores down the *c* axis in Zn_2(TTFTB), and where orange, yellow, red, and gray spheres represent Zn, S, O, and C atoms, respectively. (c) Portions of the X-ray crystal structure of Mn_2(DSBDC). View of an (–M–S–)∞ chain SBU. (d) View of infinite 1D pores along the *c* axis. H atoms and DMF molecules have been omitted for clarity.

molecules. The framework thus contains infinite (–Mn–S–) chains defined by Mn^{2+}–thiophenoxide linkages wherein the sulfur atoms at both Mn sites are oriented *trans* to each other, and where the S atoms interact with the same d orbital of Mn, thus promoting charge delocalization along the (–Mn–S–) chain (see Fig. 5b). Using the FP-TRMC derived mobility of ~ 0.02 cm^2 V^{-1} s^{-1} and the frequency of the microwave signal (9.1 GHz), the displacement length of charge carriers (defined as the distance that charge carriers can move in one oscillation of the microwave radiation) can be computed. Based on this result, the extent of charge delocaliztion in Mn_2(DSBDC) was estimated to be ~3 nm, or 8–12 (–Mn–S–) units, qualifying the framework as a Robin and Day type III system.

An alternative strategy for realizing electrical conductivity in MOFs was recently attempted by two groups who introduced guest molecules into the pores of $Cu_3(BTC)_2$ (H_3BTC = benzene-1,3,5-tricarboxylic acid) MOF thin films.[34,85] $Cu_3(BTC)_2$ is composed of binuclear copper ions coordinated by benzene tricarboxylate groups, forming a 'paddlewheel'-like structure (a common motif in MOFs, see Fig. 1, 2 and 6a). As deposited, $Cu_3(BTC)_2$ has a conductivity of $\sim 10^{-7}$ S cm^{-1}, which is most likely due to residual solvent and water present in the framework. Activated ~300 nm thick $Cu_3(BTC)_2$ films measured under inert ambient shows no measurable current ($< 10^{-12}$ A) at a bias of 10 V applied between a pair of electrodes 500 μm wide and 50 μm apart, implying a conductivity $\leq 10^{-10}$ S cm^{-1}. Dragasser *et al.* introduced ferrocene from the vapor phase into a thin film of $Cu_3(BTC)_2$ on a Au electrode and used cyclic voltammetry to deduce a conductivity of $\sim 10^{-9}$ S cm^{-1} for ferrocene@$Cu_3(BTC)_2$ films immersed in an ionic liquid.[85]

A much larger increase in conductivity was observed by Talin *et al.* who introduced TCNQ into the pores of $Cu_3(BTC)_2$.

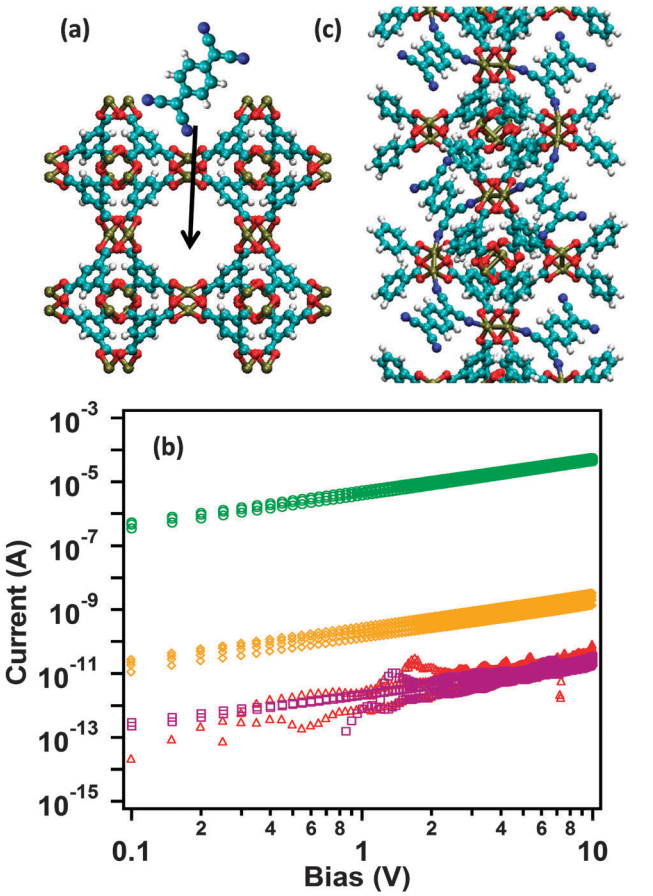

Fig. 6 (a) A TCNQ molecule shown above a $Cu_3(BTC)_2$ MOF with arrow pointing to the pore. Atom color code: white – hydrogen, blue – nitrogen, cyan – carbon, red – oxygen, ochre (light brown) – copper. (b) *I*–*V* curves before (red) and after infiltration with TCNQ (green), F_4-TCNQ (gold), or H_4-TCNQ (purple). (c) Illustration of a configuration consistent with spectroscopic data and modeling that would provide a conductive channel through the MOF unit cell.

Following adsorption of TCNQ into evacuated framework, conductivity increased to $\sim 10^{-1}$ S cm^{-1}, or an increase by at least 8 orders of magnitude (Fig. 6b) compared to the activated framework. Conductivity *versus* temperature measurements revealed thermally activated transport with a small activation energy, ~0.04 eV, similar to that observed for Berlin green. Extensive structural, spectroscopic, and modeling analysis revealed that TCNQ binds strongly to $Cu_3(BTC)_2$ when it bridges two neighboring copper paddlewheels, creating a continuous path through the MOF unit cell, as depicted in Fig. 6c. The importance of guest–host interactions on conductivity was further probed by adsorption of F_4-TCNQ, which has a higher electron affinity compared to TCNQ. This resulted in a much smaller increase in conductivity; infiltration with H_4-TCNQ, which lacks a delocalized π-network, resulted in no measurable increase in conductivity (Fig. 6b). These observations are supported by calculations using molecular clusters comprised of two copper dimer groups (MOF SBUs) bridged by a TCNQ molecule showing that: (1) binding TCNQ to the copper ions narrows the band gap by inserting unoccupied TCNQ molecular orbitals into the

HOMO–LUMO gap of the MOF. This creates a pathway for charge transfer between MOF and TCNQ. (2) Computed values of H_{AB} agree with the observed trend in conductivity with H_4-TCNQ < F_4-TCNQ < TCNQ (0.19 eV < 1.03 eV < 2.32 eV).

MOFs for light harvesting applications

MOFs present many opportunities for addressing challenges associated with light harvesting for fuel production and power generation. Extensive research in the field of luminescent MOFs supports the notion that these materials have potential for light-harvesting applications. This is a nascent area, however, and many challenges remain before practical devices can be produced that compete with state-of-the-art materials. In this section, we first review literature for two key approaches relevant to light-harvesting devices: photon capture and host–guest interactions. We follow this with a discussion of ways that MOFs can be used to promote energy transfer, which is essential for creating high-efficiency devices. Developments from research in these areas are now being translated into proof-of-concept material systems, some of which are beginning to resemble prototype devices. Overall, considerable progress has been made within the last four years, leading to our optimistic assessment that MOF-based light-harvesting devices are not far off.

In general, the characteristics that make MOFs attractive for many other applications apply here as well. However, they possess additional properties that create potential for groundbreaking improvements in these areas relative to conventional materials. In particular, compared to conventional light-harvesting organic polymers, MOFs possess long-range order that could potentially eliminate local variations known to reduce efficiency in disordered, non-crystalline PV materials.[86,87] This could lead to higher charge mobility and energy transfer rates by minimizing traps, dead ends, and defects. A related aspect is that the long-range order provided by their crystalline structure exists for multiple length scales (*e.g.*, unit cell to unit cell, pore-to-pore, guest molecule-linker orientation), suggesting possibilities to create MOF structures incorporating important features of highly evolved biological systems or complex multifunctional, but hard to control, device architectures such as dye-sensitized solar cells. The framework itself can serve as an ''active'' material that participates in energy harvesting and transfer; in this case, long-range order could persist over an entire crystal (hundreds of nanometers to tens of microns or more). Alternatively, molecular-scale order can be achieved by using the MOF pores as a venue for incorporating donor and/or acceptor species within a highly uniform environment.

MOF nanopores also enable the creation of hybrids in which the MOF structure serves one function while a separate material infiltrated into the pores, such as catalyst nanoparticles or a charge-donating or -accepting material, interacts with the framework to produce emergent properties. Additionally, these structural elements can be enhanced by functionalizing the surfaces of MOF crystals with materials such as quantum dots, redox-active quenchers, or catalysts. MOFs thus combine the best features of several ''worlds'' of electronic materials: the high order of inorganic conductors, the synthetic tunability of organic polymers, and, potentially, the ability to reduce electronic functionality to unit-cell or few-nanometer length scales, while maintaining their bulk properties. One can thus envision ''supramolecular electronics'' that address critical deficiencies of molecular electronics,[88,89] a concept that is yet to be realized.

Photon capture. The first approach to light harvesting is to use the MOF itself as the light absorber. An essential property of any active material used for light harvesting is that it must absorb solar radiation in the critical visible to near-IR region that comprises most of the photons incident upon earth. Since MOFs consist of both a metal ion and an organic linker, there are numerous possibilities for designing frameworks that can achieve this. However, many of the most common MOF compositions cannot meet this requirement. MOFs comprised of Zn(II) ions coordinated to aromatic carboxylate linkers, such as the IRMOF series, or those involving nitrogen heterocycles such as zeolitic imidazolate frameworks (ZIFs), absorb only in the UV. The Zn^{+2} d shell is full and the organic linker is usually a small molecule that is not highly conjugated. In addition, the metal–linker interaction involves very little charge transfer, as seen both experimentally[90,91] and by first-principles calculations,[92,93] leading to light absorption that is primarily ligand centered. Substituting other closed-shell metal ions, such as Cd or Mg, has little affect on these properties.[94] MOFs comprised of metal ions with open d shells, such as Co(II), Ni(II), and Cu(II), are attractive possibilities. However, there is a risk that changing the metal ion will not produce the same topology, as coordination geometries vary across the 3d group.

Consequently, modifying the electronic structure of the linker is probably a better strategy for tailoring light absorption properties. First-principles electronic structure calculations should be of help in guiding design of efficient light-harvesting MOFs. There have been a few efforts to use theory to design MOFs with appropriate visible absorption. For example, DFT tight-binding modeling of IRMOF-1 analogues indicate that the HOMO–LUMO gap can be readily tuned. By using highly conjugated, fused-ring linkers, such as perylene, the gap is predicted to decrease to ~2.6 eV.[95] Even smaller values (as low as 1.3 eV) are predicted for rather exotic linkers such as carboxylate-functionalized C_{60}. We note that the computational method used here is subject to the well-known ''band gap problem,'' in which functionals such as PBE underpredict these by as much as a factor of two. Recently, Foster *et al.* used a new non-empirically tuned, long-range-corrected DFT functional to suggest a modular series of linker molecules that have electronic properties and structures suitable for visible light harvesting. These linkers are adapted for the MOF-74 topology and are based on alternating electron-deficient benzo[*c*][1,2,5]thiadiazole (BT) and electron-rich thieno[3,2-*b*]thiophene (TT) moieties. The new DFT functional models charge transfer and Rydberg states with much greater accuracy than conventional pure and hybrid functionals such as B3LYP.[96] The results demonstrate that the fundamental and optical gaps of MOF-74 can be readily tuned to achieve orbital alignments with electron acceptors such as PCBM (Fig. 7). Because these new linkers preserve the carboxylate–oxo coordinating groups used in the IRMOF-74 series, their electronic

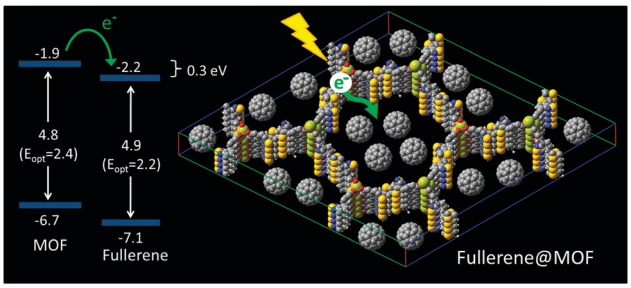

Fig. 7 Schematic showing the HOMO and LUMO orbital alignment (left) with C_{60} of a TT–BT–TT linker (see text) in an IRMOF-74 topology (right). Adapted from ref. 96.

structure remains largely unaffected by the metal ion. Consequently, their absorption spectra in dilute solution can be used to benchmark the accuracy of the DFT method. Good agreement is found, showing that synthesis of MOFs with these types of linkages can be effectively guided by using these more accurate theoretical methods prior, to attempting a potentially difficult synthesis effort.

Guest molecules and composite MOFs. A second approach to improving light capture by MOFs is to infiltrate the pores with light-absorbing guest molecules. Streit *et al.* grew thin films of the MOF HKUST-1 and used solution infiltration to load the pores with a europium β-diketonate complex.[97] This MOF absorbs strongly in the UV and more weakly in the 400–550 nm region. Excitation of the MOF linker at ~275 nm produces emission characteristic of the europium complex at 615 nm, demonstrating that the MOF can act as a sensitizer that broadens the absorbance. In this case, the mechanism appears to be Dexter energy transfer, since the MOF is not fluorescent and thus cannot engage in fluorescence resonance energy transfer (FRET). The Dexter mechanism is a quantum-mechanical phenomenon involving direct interaction of the electron clouds of the donor and acceptor moieties. Based on the shape of the excitation spectrum, these authors conclude that the transfer is between the btc linker of the MOF and the 1-benzoylacetone ligand of the europium complex. MOFs as hosts, active or passive, for a variety of other species have been reported. For example, incorporating fluorescent dye molecules into IRMOF-1 results in blue-shifted emission and energy transfer from the linker to the dye molecule.[98] Charge-transfer complexes can also be formed between a MOF having an electron-accepting linker, as seen in the work by Takashima *et al.*, in which dipyridylnaphthalenediimide linkers in the MOF accept charge from guest electron donors such as amines.[99] Here, the light-absorbing properties, manifested by a CT band, can be tuned across the visible portion of the spectrum.

The concept of the MOF as sensitizer for guest molecules was extended to donor and acceptor molecules typically used in organic photovoltaic devices. Leong *et al.* employed MOF-177, a large-pore MOF consisting of Zn^{+2} coordinated to benzenetribenzoate (btb) linkers, as a nominally "passive" host for donor thiophene oligomers and acceptor [6,6]-phenyl-C61-butyric acid methyl ester (PCBM) molecules.[100] This guest–MOF combination serves as a first step toward creating a "nano-heterojunction," in which the MOF eliminates disorder inherent in conventional bulk heterojunction (BHJ) devices composed of molecular and/or polymer organic semiconductors. The thiophene loading achieved was very light, ~1 molecule of α,ω-dihexylsexithiophene (DH6T) per 11 unit cells, due to the steric constraints associated with the length of the thiophene molecule. Much heavier PCBM loadings (2.5 PCBM per unit cell; ~22 wt%) were achieved, which are comparable to those used in BHJ solar cells. Remarkably, however, no evidence of phase segregation was observed, demonstrating that reduced disorder in donor–acceptor pairs can be achieved using MOFs. Excitation at 345 nm, which pumps the btb linker, produced efficient fluorescence resonance energy transfer (FRET) with both guest molecules. The btb emission was quenched by both guest molecules. When the quencher was DH6T, luminescence from that guest appeared (PCBM is not luminescent, so no new luminescence was observed), showing that the MOF behaves as a photon antenna. With both guests present, even greater quenching was observed, likely due in part to an "FRET cascade", *i.e.* sequential MOF-177 → DH6T → PCBM energy transfer (Fig. 8). Although unfavorable band alignment for actual charge transfer was predicted from DFT calculations, interestingly, this could not be fully ruled out. Time-dependent DFT calculations applied to the first 100 excited states revealed that btb-to-PCBM charge transfer (CT) states exist. However, analogous btb-to-DH6T CT states were not predicted, although the position of the btb LUMO ~ 0.35 eV above the DH6T LUMO indicates this should be possible. Overall, the results demonstrate that MOFs can be multifunctional hosts that possess both photon harvesting properties and the ability to reduce disorder that is a serious issue in conventional BHJ materials.

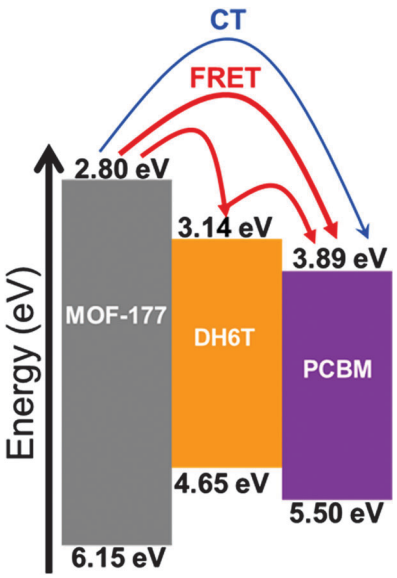

Fig. 8 MOF-177, DH6T & PCBM band alignment predicted by SCC-DFTB, showing the possibility of either a FRET cascade and charge transfer from MOF-177 to PCBM. From ref. 100.

Nanoparticles of metal oxides such as TiO_2 used in dye-sensitized solar cells and as photocatalysts can also be incorporated into MOFs. For example, Fischer and coworkers formed nanoscale titania particles within IRMOF-1. Although clear evidence from electron microscopy is lacking, their results indicate that nanoscale titania particles can be formed with properties similar to surfactant-stabilized TiO_2.[101] The emission of these particles can be tuned using the time and temperature of annealing. In an interesting extension of this concept, Lu *et al.* incorporated surfactant-modified nanoparticles of various shapes (CdTe, Pt, and La-doped $NaYF_4$ nanorods) within ZIF-8 crystals without the agglomeration that occurs in solution.[102] In this case, the objective was not to use the MOF as a template, but rather to create a spatially ordered composite material. The high degree of control over the nanoparticle location within the MOF crystal is remarkable and was achieved by adding the particles at different times during the ZIF-8 growth process (Fig. 9). These composite materials combine the sieving behavior of the MOF crystal with functionalities such as catalysis, magnetism, and photoluminescence, suggesting this could be a facile method for incorporating nanoparticles into a variety of MOF-containing electronic device structures.

Another kind of MOF composite can be made by functionalizing the surfaces of the MOF crystals themselves. Recently, this was achieved by coating porphyrin-based MOF crystals with a monolayer of semiconductor quantum dots (SQD). These act as sensitizers, transferring energy to the MOF by relatively efficient Förster energy transfer (>80%). The resulting hybrid material harvests light efficiently over a broad spectral range.[103] A one-pot method for incorporating core–shell quantum dots into the IRMOF-1 structure was also reported.[104] The resulting highly luminescent composite material behaves as a size-selective molecular sensor.

Energy transfer. Long-distance energy transfer may be required if thick absorber films are needed to efficiently capture available photons. There are now a number of examples showing that MOFs present a unique possibilities for solving the problem of high-efficiency, long-distance energy transfer. The group of Wenbin Lin has explored these possibilities, beginning with the synthesis of mixed Ru^{II}–Os^{II} MOFs with bipyridyl ligands. These molecules have metal-to-ligand charge transfer (MLCT) excited states that can be used to probe site-to-site energy transfer. The presence of the heavy metal ion also leads to increased spin–orbit coupling, allowing the energy of excited triplet excitons that are normally non-emissive to be harvested productively. This is a well-known concept in organic light-emitting diodes (OLEDs).[105] Using transient emission decay profiles, Kent *et al.* determined that a Ru excited state can hop 15–55 times over its lifetime, corresponding to distances of 15–55 nm.[106] This concept proved useful not only in energy transfer, but as a diagnostic platform for probing molecular diffusion in solvent-filled MOF pores.[107] Building on this platform, Kent *et al.* constructed MOFs from photoactive Ru(II)-(bpy) building blocks that are strong visible absorbers. Using both oxidative and reductive quencher molecules, they were able to show that long-distance energy transfer (over several hundred nm) occurred, monitoring this by the

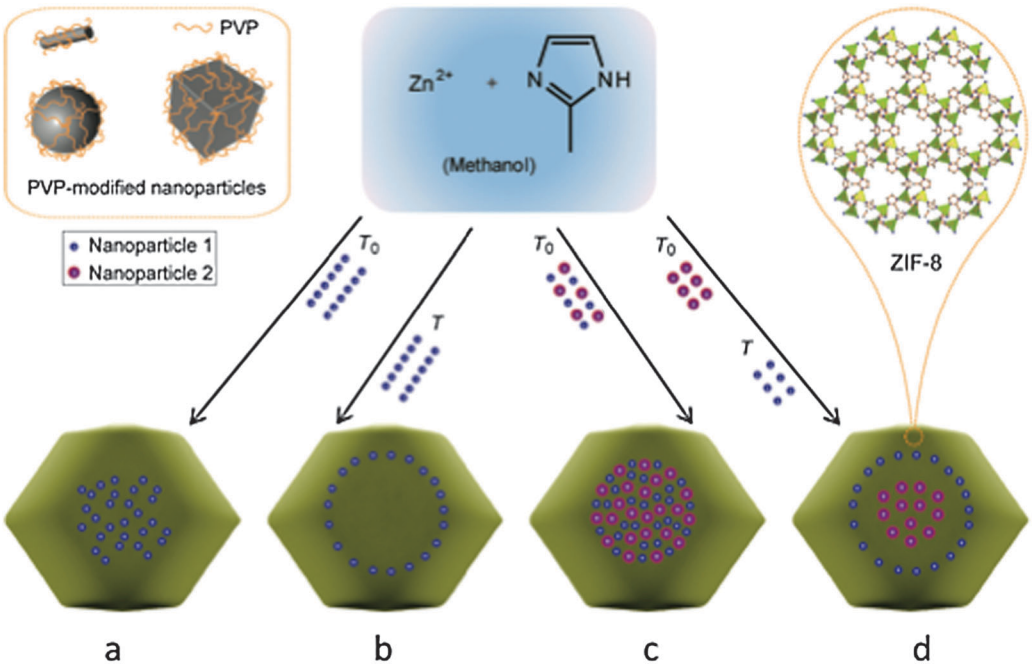

Fig. 9 Method for controlled encapsulation of nanoparticles in ZIF-8 crystals. Surfactant-functionalized nanoparticles of various types are encapsulated within ZIF-8 crystals. Spatial distribution is controlled by adjusting the time of addition to the solution from which ZIF-8 is crystallizing. Examples of achievable spatial distributions include the following: nanoparticles of a single type in the central area (a) or off the central area (b) of the ZIF-8 crystals; as two types of nanoparticles in the central areas (c) or one type in the central area, but the other type in the transition layers (d) of the MOF crystals. Adapted from ref. 102.

efficient electron-transfer quenching at the MOF-solution interface.[106] Recent theoretical investigations show that this triplet migration occurs by an incoherent hopping mechanism involving Dexter energy transfer.[108] Observed rates of energy transfer (again measured by quenching studies) can be more than one hundred times higher than the diffusion-controlled limit. Moreover, the quenching is amplified by 7000-fold relative to a model complex in solution. These results show that "outer-sphere" electron transfer is feasible in a MOF, a concept with links to biological redox systems. This suggests that the combination of long-range crystalline order in MOFs and their synthetic tunability can be used to design systems that couple light harvesting with fast energy transport for efficient electrochemistry at crystal surfaces.

A different approach is being implemented by Hupp and coworkers, in which light harvesting and energy transfer are implemented using porphyrin-based MOFs. These authors designed multi-linker structures that incorporate donor and acceptor functionalities within the framework. A pillared-paddlewheel MOF, combining a symmetrical Zn-porphyrin (ZnPor) with an emissive pyridine-functionalized boron dipyrromethene (bodipy) pillar, provided broad coverage across the visible region. Due to spectral overlap between bodipy emission and ZnPor absorption, near-quantitative energy transfer from bodipy to ZnPor is observed *via* a FRET mechanism (Fig. 10).[109] A subsequent report revealed that minor modifications of the porphyrin linker can lead to fast, anisotropic exciton hopping. Specifically, reducing the symmetry of the porphyrin linker by the addition of two coaxial acetylene groups leads to increased π-conjugation and higher oscillator strength of the porphyrin Q-band absorption. Since the strength of the absorption is directly related to the exciton hopping rate by Förster energy transfer, exciton coupling is increased, resulting in hopping about an order of magnitude faster than in an analogous MOF constructed from a porphyrin linker without these groups.[110] This strategy is reminiscent of approaches used to improve spectral coverage and energy transfer in dye-sensitized solar cells (DSSC). Although head-to-head comparisons with state-of-the-art light-harvesting organics have not yet been made, the potential for rational design with long-range order presents a distinct advantage for MOFs in these applications.

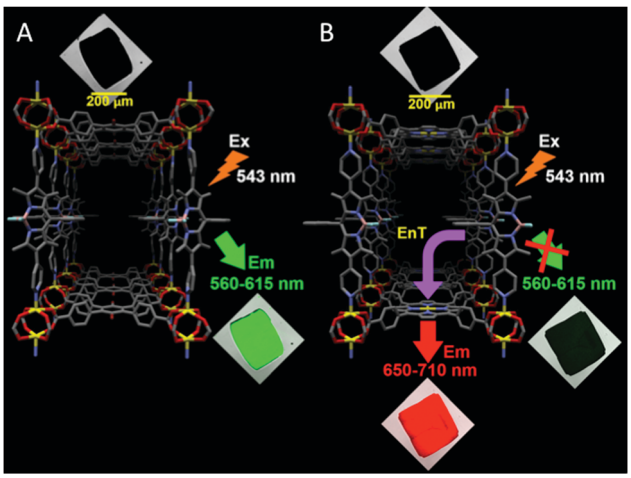

Fig. 10 Confocal laser scanning microscopy illustrates the effective strut-to-strut energy transfer. In (A), a MOF comprised of non-emissive dibromo-tetrakiscarboxyphenyl linkers and emissive bodipy linkers produces 560–615 nm emission characteristic of the bodipy linker when irradiated at 543 nm, where it linker absorbs strongly. In contrast (B), a second MOF, comprised of a symmetrical carboxyphenyl porphyrin and bodipy linkers emits light characteristic of the porphyrin due to efficient FRET from bodipy to the porphyrin. Adapted from ref. 109.

Applications. Examples of MOFs being used as active materials for either photocatalysis or in photovoltaic cells (PVC) are limited but intriguing. Considering their use as PV active materials, a clear requirement beyond light absorption is charge mobility, a characteristic that is not necessary for a MOF to behave as a photocatalyst. For current generation, photo-generated carriers (electrons and holes) must be able to move through the material, either under the influence of an internal field, as would be imposed by the junction of p- and n-type semiconductors, or as a result of an applied voltage. As discussed above, there are very few MOFs that behave as semiconductors, which exhibit dispersion in their ground and excited state electronic band structure. Most MOFs, in contrast, exhibit localized electronic structure, with little mixing between the metal ion atomic orbitals and the linker molecular orbitals. This is particularly true of MOFs composed of Zn^{2+} ions, where the filled 3d shell prevents ligand-to-metal charge transfer (metal-to-ligand charge transfer is possible, but occurs at energies well outside the visible region of the spectrum for the types of linkers typically used in MOFs). Both spectroscopic data[90,111] and theoretical predictions of MOF band structure[92] and density of states support this notion. As a result, it is inaccurate to refer to conduction and valence bands in these materials. Claims of semiconducting behavior by, for example, IRMOF-1[112] and photocurrent production by devices incorporating $Al_2(bdc)_3$[113] must therefore be viewed with some skepticism. Although these MOFs can absorb light in the UV, the resulting exciton remains a bound charge pair, rather than undergoing charge separation as would occur in a doped semiconductor or in an organic bulk heterojunction.

The photocurrent produced by PV cells incorporating the MOF $Al_2(bdc)_3$ is an interesting observation, however, as it suggests a possible role for MOFs in DSSC devices. Lopez *et al.* fabricated photovoltaic cells by depositing a layer of the MOF, prepared as a paste, on top of a 20 nm thick film of dense TiO_2 hole blocking layer on an ITO substrate.[113] A hole-conducting material was then spun on, followed by deposition of gold contacts. This configuration is not unlike a DSSC, but it lacks the dye-regenerating electrolyte. It therefore seems possible that the MOF is acting as a sensitizer for TiO_2. Interestingly, the highest photocurrent was found for MOF films infiltrated with the electron-donating guest molecule dimethoxybenzene, which may play a role in regenerating the MOF following photoexcitation. Photocurrent decreased with increasing layer thickness (several microns), suggesting light blocking and/or inhibition of charge transport. Other investigators have proposed using MOFs in various roles within a DSSC. There is some evidence for an improvement in open circuit voltage (V_{OC}) when TiO_2 is

coated with a layer of ZIF-8.[114] Coating thicknesses of ~2 nm increase V_{OC} by up to 66 mV, with V_{OC} increasing as the ZIF-8 thickness increases. The mechanism of this improvement appears to be the inhibition of interfacial charge recombination.[114] Although far from conclusive, these efforts bring new design potential to DSSC and are worthy of further exploration.

The conclusions regarding photocurrent generation do not preclude the possibility of MOFs behaving as photocatalysts. There are now several examples in which absorption of light generates reducing electrons or oxidizing holes in the near-surface region of MOF crystals in solution. Catalyst regeneration in this case can occur by reaction with a secondary reactant in the solution. Gascon and colleagues showed photoinduced oxidation of propylene to acrylic acid, for example, using IRMOF-1 as a platform for tuning the optical gap by varying the organic linker.[115] MOFs with narrower optical gap (*e.g.*, IRMOF-8 with 2,6-naphthalenedicarboxylate linkers and a measured optical gap of 3.3 eV) were the most effective, whereas IRMOF-1 (measured optical gap of 4.0 eV) showed no activity. This group also functionalized MIL-125(Ti) with red-absorbing dye molecules (attaching them to primary amines on the linkers), broadening the spectrum of absorbed light and increasing the turnover rate of benzyl alcohol oxidation to benzaldehyde.[116] Tachikawa *et al.* found that IRMOF-1 nanoparticles are more efficient photo-oxidation catalysts than P-25 TiO_2 powder, a common photocatalyst. Green photoluminescence (PL) produced by the nanoparticles is similar to ZnO, but the temperature dependence of the PL is quite different, increasing up to 170 K, then decreasing at higher temperatures.[117] The reason for this behavior is unclear, but appears to be related to multiple defect types.

These examples of MOF-based photocatalysis suggest possibilities of their use in selective synthesis of small molecules, but are also conceptually promising for solar-generated fuel production. To that end, Lin and coworkers prepared MOF-based catalysts by incorporating complexes of Ir, Re, and Ru into the UiO-67 framework.[118] This work shows how molecular catalysts can be combined with MOFs to improve catalyst performance and stability. The Re-derivatived MOF catalyzes CO_2 reduction with a turnover frequency three times higher than the analogous Re complex in solution. The UiO-67 MOF is advantageous for this reaction because of its high thermal stability and inertness in aqueous solution. Extending these concepts, they loaded Pt nanoparticles into a framework comprised of two different building blocks (Fig. 11): photocatalytic Ir(ppy)(bpy) dicarboxylates (ppy = 2-phenyl pyridine; bpy = 2,2′-bipyridine) and inert $Zr_6(\mu_3\text{-}O)_4(\mu_3\text{-}OH)(carboxylate)_{12}$ groups.[119] An interesting aspect of this synthetic strategy is that matching the lengths of these two ligands allows facile substitution and controlled doping of the Ir complex for the Zr-carboxylate linker. Pt nanoparticles were created by photoreduction of a Pt salt infiltrated into the pores, using a strategy similar to that developed by Fischer *et al.*[120] Triethylamine was used as a mediator to reductively quench the photo-induced triplet state of the Ir complex, creating a radical that transfers electrons to the Pt nanoparticles, which then reduce H_2O to make H_2. The observed enhancement of the photocatalytic H_2 evolution is thought to be due to more efficient

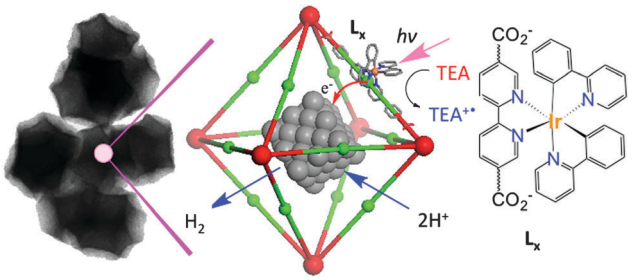

Fig. 11 A phosphorescent MOF comprised of organometallic iridium and phenylpyridine subunits were loaded with Pt nanoparticles. The resulting assembly acts as a photocatalyst: $Ir(ppy)_2(bpy^{\bullet -})$ radicals, created by the light-absorbing MOF (using triethylamine mediator), are injected into the nanoparticles, which then transfer them to protons to produce H_2. Adapted from ref. 119.

electron transfer from the Ir complex to the Pt nanoparticles. Degradation of the Ir catalyst was also reduced relative to the same reaction in solution, suggesting that the complex is more chemically inert. These results are highly encouraging, illustrating the aspects of MOFs that make them unique for photocatalysis applications relative to other photoactive materials, such as organic polymers and porous semiconducting oxides.

MOFs in sensors

The principle of solid-state sensor devices is based on their transduction mechanism (mass, optical, acoustic, magnetic, or electric changes) to the chemical environment, *i.e.* the intrinsic properties of the active materials are influenced by the presence of analyte molecules. The chemical, physical or structural changes in a MOF upon adsorption of guest molecules have been utilized in recent years for the detection of various chemical species. A comprehensive review article on MOFs for sensing applications was published in 2011.[11] Here we focus on developments in this field since this review appeared.

Our group implemented MOF thin films with microcantilevers and Surface Acoustic Wave (SAW) devices for small molecule detection.[121–124] $Cu_3(btc)_2$-functionalized SAW sensors exhibit sensitivity to water vapor from 0.28 to 14 800 ppmv, which exceeds the sensitivity or range of many commercial sensors. Sensor response as a function of MOF coating thickness was evaluated, showing that SAW sensor response is bounded by maximum and minimum layer thicknesses. Microfabricated cantilever sensors can be used to detect small molecules and volatile organic compounds (VOCs) based on chemically induced strain. HKUST-1 coated piezoresistive microcantilevers, previously shown to respond reversibly to water, methanol, and ethanol, were recently shown to also respond to various hydrocarbons, including acetone, chloroform and toluene. The concentration range of the analytes that can be detected by this technique varies in a wide range, from tens to thousands of ppm. The MOF-coated microcantilevers did not respond to hexamethyldisiloxane, 1,2-dichloroethane, and CO_2, but did detect *n*-hexane and *n*-decane, although the response was reversible only after baking in dry nitrogen. Characteristic response features allow discrimination based on shape, response time constants, and magnitude of response for various VOCs. MOF-coated

microcantilever devices are robust and in selected cases provided reliable and reversible sensor response over 18 months of testing. In this context, Venkatasubramanian *et al.* explored MOF coating properties and microcantilever design to optimize this sensing platform.[124] Very recently, Tu and Fischer assembled a dual-component SURMOF heterostructure on QCM electrodes, which can be used to selectively adsorb volatile organic compounds, such as methanol, 1,3,5-trimethylbenzene and 1,3,5-triisopropylbenzene. The change in mass of the SURMOF bilayer is based of two lattice-mismatched components, with $[Cu_3(btc)_2]$ grown on top of $[Cu_2(ndc)_2(dabco)]$. The resulting highly oriented, continuous films are assembled using layer-by-layer liquid-phase heteroepitaxy.

S. Kitagawa and co-workers demonstrated a binary "Janus MOF" (Janus = system with two or more different physical or chemical properties) composed of tetragonal pillared-type MOFs: A = $[Cu_2(ndc)_2(dabco)]$ and B = $[Cu_2(NH_2\text{-}bdc)_2(dabco)]$ (Fig. 12), where ndc = 1,4-naphthalenedicarboxylate; NH_2-bdc = 2-amine-1,4-benzenedicarboxylate; dabco = 1,4-diazabicyclo-[2.2.2]-octane.[13] Framework B was further post-synthetically modified with succinic acid anhydride to form C = $[Cu_2(HOOC(CH_2)_2OCNH\text{-}bdc)(NH_2\text{-}bdc)(dabco)]$. Fig. 4 shows the different types of coatings synthesized on pyridyl-terminated SAMs. Janus PCP coating of type I(C@A) or type II(A@C) were built from the frameworks A and B, grown epitaxially on top of each other, whereas type III(AC) followed by conversion of B to C through postsynthetic acylation of the amine group. Type III(AC) coatings consisted of statistically distributed apolar and polar ligands without spatial separation of distinct PCP systems. All three types of MOF coatings were deposited on the gold surfaces of QCM sensors that were modified by pyridyl-terminated self-assembled monolayers to achieve selective gas uptake.

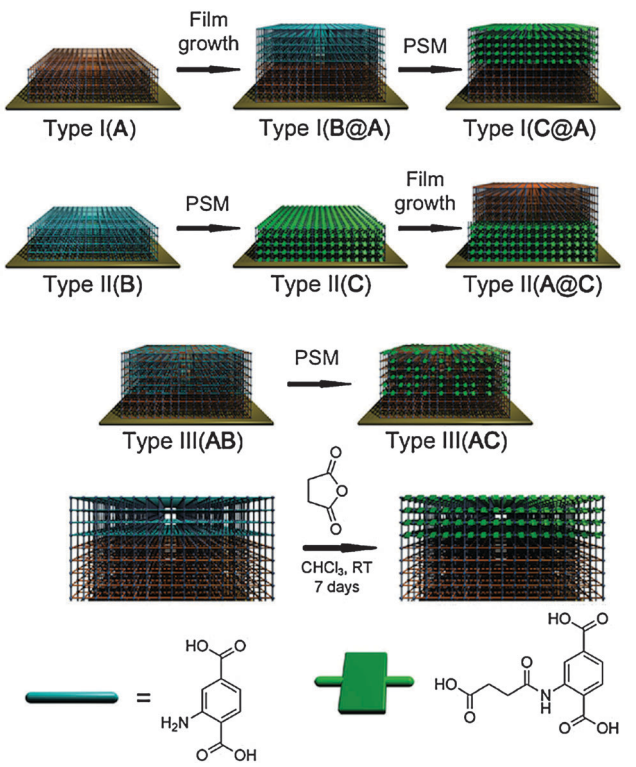

Fig. 12 Different types of heterostructured Janus PCP coatings with PCP frameworks A: $[Cu_2(ndc)_2(dabco)]_n$; B: $[Cu_2(NH_2\text{-}bdc)_2(dabco)]_n$; C: $[Cu_2(HOOC(CH_2)_2OCNH\text{-}bdc)_2(dabco)]_n$ and the principle of post-synthetic modification of Janus PCP coatings demonstrated for type I(B@A) material. Adapted from ref. 13.

The optical and luminescent properties of MOFs make them promising as active layers in chemical sensors.[11,12] Since photoexcitation of a typical MOF linker populates the LUMO with a strongly reducing electron leaving a highly oxidizing hole in the linker's HOMO, the luminescence of many MOFs can be attenuated by adsorption of redox active molecules. Several excellent reviews on the topic of luminescent MOFs appeared over the last few years.[27–29] Here, we report a few representative examples from recent literature, with the emphasis on selective analyte detection.

Lin *et al.* reported a chiral fluorescent metal–organic framework (MOF) based on Cd(II) 2,2′-dihydroxy-1,1′- binaphthyl-4,4′,6,6′-tetrakis(4-benzoate). The MOF was proposed as an enantioselective sensor for amino alcohols *via* fluorescence quenching. The fluorescence was quenched by several chiral amino alcohols with good enantioselectivity. The highest enantiomeric quenching ratio of 3.12 was observed for 2-amino-3-methyl-1-butanol. The fluorescence quenching of this chiral MOF was attributed to the H-bonding between amino alcohols and the binaphthol moieties decorating the MOF. A pre-concentration effect inside the MOF channels increased detection sensitivity, whereas the higher enantioselectivity of the MOF was attributed to the enhanced chiral discrimination due to the cavity confinement effect and the conformational rigidity of the liner moieties in the framework.

Tang *et al.* reported a piperidine-based MOF, $[Eu(BTPCA)(H_2O)]\cdot 2DMF\cdot 3H_2O$ (H_3BTPCA = 1,1′,1″-(benzene-1,3,5-triyl)tripiperidine-4-carboxylic acid), which can be successfully used to detect Fe^{3+} and Zn^{2+} cations (Fig. 13).[125] The triazinyl N atoms of the ligand are directed into the channels of the framework and are believed to favor interactions with metal cations. These donor–acceptor interactions alter the electronic structure of the BTPCA ligand that mediates the ligand-to-Eu^{3+} energy transfer and determines the luminescence of the lanthanide ion. When exposed to Fe^{3+}, the red luminescence of the $^5D_0 \rightarrow {}^7F_2$ transition (618 nm) was completely quenched. In contrast, the interaction with Zn^{2+} enhances the luminescence intensity by a factor of 3.5 compared to the parent MOF. Other metal cations were tested, including K^+, Al^{3+}, Cr^{3+}, Mn^{2+}, Co^{2+}, Ni^{2+}, and Cu^{2+}, however no significant changes were observed. Chen and co-workers reported a different Eu-based MOF, namely $[Eu(PDC)_{1.5}(DMF)]\cdot 0.5DMF\cdot 0.5H_2O$ (PDC = pyridine-3,5-dicarboxylate), which show a "turn-off" response to Mn^{2+}, Co^{2+} and Cu^{2+}. The metal binds to the pyridyl N atoms of the PDC ligand, which leads to a weaker antenna effect.

Although the vast majority of luminescent-based MOF sensors operate through the "turn-off" mechanism, recently S. Kitagawa and co-workers proposed an entangled MOF structure, $[Zn_2(bdc)_2(dpndi)]_n$, (bdc = 1,4-benzenedicarboxylate; dpndi = *N*,*N*′-di-4-pyridyl-1,4,5,8-naphthalenediimide), which shows enhancement in fluorescence upon analyte adsorption.[99,126]

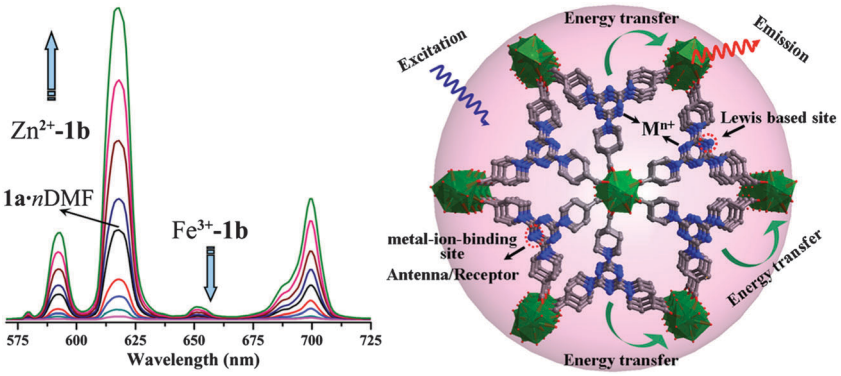

Fig. 13 Schematic representation fluorescence-based sensing of Fe^{3+} and Zn^{2+} by [Eu(BTPCA)(H_2O)]·2DMF·3H_2O. Adapted from ref. 125.

When exposed to selected aromatic organic compounds, such as benzene, toluene, xylenes, anisole and iodobenzene, the entangled framework displays a crystal-to-crystal phase transition. The structural change is accompanied by a strong and analyte-specific enhancement of fluorescence. This is a rare example of "turn-on" fluorescence and two mechanisms are believed to be responsible for the observed guest-molecule selectivity: (1) charge-transfer emission and (2) heavy-atom-induced phosphorescence enhancement. Another example of the "turn-on" luminescence mechanism triggered by organic solvent molecules was reported by Li *et al.* on a luminescent europium(III) MOF.[127] The water-exchanged MOF, [$Eu_2L_3(H_2O)_4$] (L = 2′,5′-bis(methoxymethyl)-[1,1′:4′,1″-terphenyl]-4,4″-dicarboxylate), display characteristic emissions at 578, 590, 616, and 698 nm, corresponding to $^5D_0$–$^7F_0$, $^5D_0$–$^7F_1$, $^5D_0$–$^7F_2$, and $^5D_0$–$^7F_4$ transitions of Eu(III). Upon exposing the MOF to DMF vapor, the luminescence increases and reaches an eightfold enhancement when fully saturated. A prototype sensor was fabricated and shows a response time to DMF of the order of a few minutes. The active sensing material can be regenerated by soaking in water and reused in detection experiments without notable loss of the selectivity upon cycling. Other solvents tested include Me_2CO, Et_2O, THF, CH_2Cl_2, EtOAc, MeOH, EtOH, MeCN, formamide, C_6H_6 and hexanes, however only modest enhancements (<2 times) in luminescence were observed. The luminescence lifetime studies revealed that the "turn-on" MOF response to DMF is due to DMF–linker interactions that shift the excited state energy level of the organic linker leading to an improved antenna effect.

Selective MOF growth on a desired surface is necessary for certain sensor types, but is not yet routine. However, recent proof-of-concept studies show that in principle this is feasible. Thus, Hupp and co-workers fabricated patterned ZIF-8 thin films using standard photolithography and *via* selective MOF growth with the aid of microcontact printing.[102] The alternate chemical deposition (of ZIF-8) and physical deposition (of metallic materials) allow the insertion of metal layers in the ZIF-8 film that could serve as multifunctional chemical sensors for vapors and gases. The optical properties of multilayered MOF–palladium hybrid structures are capable of behaving as sensors for selective detection of various gases, including hydrogen, ethane, ethylene, propane, and propylene. More recently, S. Kitagawa and co-workers fabricated thin films of NH_2-MIL-53(Al), ZIF-67 and ZIF-8 using a common epoxy-based photoresist (SU-8) by UV lithography coupled with an imprinting technique.[128] The method consists of imprinting the photoresist film into a film of MOF powder, which yields a patterned MOF film. The patterning approaches represent an important step towards highly functionalized MOFs,[129] and are potentially useful for commercial applications such as lab-on-a-chip type devices.

Conclusions and outlook

This review illustrates some of the many emerging opportunities for using MOFs in electronic and optoelectronic devices. Their combination of long-range order and synthetic flexibility, manifested by the presence of both metal ions and organic linkers in a predetermined spatial orientation, enables a wide range of tunable properties useful in functional devices. Although the field of MOFtronics is very new, recent demonstration of several device types in which a MOF plays an active role is encouraging, including light-harvesting devices and sensors based on various transduction mechanisms. Unfortunately, electrically conducting MOFs are still a rarity. Although the structural properties of MOFs undoubtedly determine charge carrier mobility, the mechanisms responsible for conductivity in organic materials are in general poorly understood. As a result, sensors incorporating MOF-based recognition chemistries are currently the most promising candidate for commercial applications, with performance comparable to state-of-the-art commercial devices achieved at least in one case (water vapor detection).

Significant progress in the last few years concerning the integration of MOF films with micro- and even nanoscale device architectures is encouraging, but commercial tools for depositing MOF films are not yet available. Although several new methods for depositing uniform, oriented MOF films have been developed recently, fast wide-area growth, defect control, and precise lithographic patterning must become possible if MOFs are to realize their potential as a novel class of electronic materials. Generic processing techniques that provide control of composition, thickness, and functionality of a broad range of MOF films must be developed. In addition, the mechanical and environmental

stability of MOFs is poorly characterized. These challenges highlight the need for MOF research to expand beyond the realm of synthetic inorganic chemistry and become the focus of research by those with expertise in solid-state physics and device engineering, as well as attracting the attention of individuals with expertise in lithography, process design, and materials integration. Nevertheless, activity in this area of chemistry continues to increase, raising the likelihood that interdisciplinary efforts will be germinated soon.

Acknowledgements

This work was supported by the Laboratory Directed Research and Development Program at Sandia National Laboratories and the U.S. DOE SunShot Program. Sandia is a multi-program laboratory operated by Sandia Corporation, a Lockheed Martin Company, for the U.S. DOE National Nuclear Security Administration under Contract DE-AC04-94AL85000. AAT was supported in part by the Science of Precision Multifunctional Nanostructures for Electrical Energy Storage (NEES), an Energy Frontier Research Center funded by the U.S. DOE, Office of Science, Office of Basic Energy Sciences under award DESC0001160.

References

1 *Metal Organic Frameworks: Applications from Catalysis to Gas Storage*, ed. D. Farrusseng, Willey-VCH, 2011.
2 *Functional Metal-Organic Frameworks: Gas Storage, Separation and Catalysis*, ed. M. Schröder, Springer, Berlin, Heidelberg, 2010.
3 *Metal-Organic Frameworks: Design and Applications*, ed. L. R. MacGillivray, Wiley-VCH, 2010.
4 H. X. Deng, S. Grunder, K. E. Cordova, C. Valente, H. Furukawa, M. Hmadeh, F. Gandara, A. C. Whalley, Z. Liu, S. Asahina, H. Kazumori, M. O'Keeffe, O. Terasaki, J. F. Stoddart and O. M. Yaghi, *Science*, 2012, **336**, 1018.
5 H. Furukawa, K. E. Cordova, M. O'Keeffe and O. M. Yaghi, *Science*, 2013, **341**, 974.
6 N. L. Rosi, J. Kim, M. Eddaoudi, B. L. Chen, M. O'Keeffe and O. M. Yaghi, *J. Am. Chem. Soc.*, 2005, **127**, 1504.
7 O. M. Yaghi, M. O'Keeffe, N. W. Ockwig, H. K. Chae, M. Eddaoudi and J. Kim, *Nature*, 2003, **423**, 705.
8 J. A. Mason, M. Veenstra and J. R. Long, *Chem. Sci.*, 2014, **5**, 32.
9 J. R. Li, R. J. Kuppler and H. C. Zhou, *Chem. Soc. Rev.*, 2009, **38**, 1477.
10 S. T. Meek, J. A. Greathouse and M. D. Allendorf, *Adv. Mater.*, 2011, **23**, 249.
11 L. E. Kreno, K. Leong, O. K. Farha, M. Allendorf, R. P. Van Duyne and J. T. Hupp, *Chem. Rev.*, 2011, **112**, 1105.
12 M. D. Allendorf, A. Schwartzberg, V. Stavila and A. A. Talin, *Chem. – Eur. J.*, 2011, **17**, 11372.
13 M. Meilikhov, S. Furukawa, K. Hirai, R. A. Fischer and S. Kitagawa, *Angew. Chem., Int. Ed.*, 2013, **52**, 341.
14 D. Di Sante, A. Stroppa, P. Jain and S. Picozzi, *J. Am. Chem. Soc.*, 2013, **135**, 18126.
15 C. Pan, J. Nan, X. Dong, X.-M. Ren and W. Jin, *J. Am. Chem. Soc.*, 2011, **133**, 12330.
16 P. Canepa, Y. J. Chabal and T. Thonhauser, *Phys. Rev. B: Condens. Matter Mater. Phys.*, 2013, **87**, 094407.
17 T. Gao, X.-Z. Wang, H.-X. Gu, Y. Xu, X. Shen and D.-R. Zhu, *CrystEngComm*, 2012, **14**, 5905.
18 Q. Zhang, B. Li and L. Chen, *Inorg. Chem.*, 2013, **52**, 9356.
19 W. Zhenxing, P. Jain, C. Kwang-Yong, J. van Tol, A. K. Cheetham, H. W. Kroto, H. J. Koo, Z. Haidong, H. Jungmin, C. Eun Sang, W. Myung-Hwan and N. S. Dalal, *Phys. Rev. B: Condens. Matter Mater. Phys.*, 2013, **87**, 224406.
20 S. Eslava, L. Zhang, S. Esconjauregui, J. Yang, K. Vanstreels, M. R. Baklanov and E. Saiz, *Chem. Mater.*, 2012, **25**, 27.
21 E. Redel, Z. Wang, S. Walheim, J. Liu, H. Gliemann and C. Wöll, *Appl. Phys. Lett.*, 2013, **103**, 091903.
22 K. Zagorodniy, G. Seifert and H. Hermann, *Appl. Phys. Lett.*, 2010, **97**, 251905.
23 J. M. Taylor, K. W. Dawson and G. K. H. Shimizu, *J. Am. Chem. Soc.*, 2013, **135**, 1193.
24 M. Yoon, K. Suh, S. Natarajan and K. Kim, *Angew. Chem., Int. Ed.*, 2013, **52**, 2688.
25 S. Horike, D. Umeyama and S. Kitagawa, *Acc. Chem. Res.*, 2013, **46**, 2376.
26 A. Morozan and F. Jaouen, *Energy Environ. Sci.*, 2012, **5**, 9269.
27 M. D. Allendorf, C. A. Bauer, R. K. Bhakta and R. J. T. Houk, *Chem. Soc. Rev.*, 2009, **38**, 1330.
28 Y. Cui, Y. Yue, G. Qian and B. Chen, *Chem. Rev.*, 2011, **112**, 1126.
29 J. Heine and K. Mueller-Buschbaum, *Chem. Soc. Rev.*, 2013, **42**, 9232.
30 W. Lili, Z. Li, Z. Bingguang, M. Xianggao, Q. Hua and L. Dongfeng, *J. Mater. Chem.*, 2012, **22**, 22603.
31 C. Lin, H. Huayou, Z. Liming and G. Shaohua, *Inorg. Chem. Commun.*, 2012, **15**, 202.
32 D. M. D'Alessandro, J. R. R. Kanga and J. S. Caddy, *Aust. J. Chem.*, 2011, **64**, 718.
33 C. G. Silva, A. Corma and H. Garcia, *J. Mater. Chem.*, 2010, **20**, 3141.
34 A. A. Talin, A. Centrone, A. C. Ford, M. E. Foster, V. Stavila, P. Haney, R. A. Kinney, V. Szalai, F. El Gabaly, H. P. Yoon, F. Leonard and M. D. Allendorf, *Science*, 2014, **343**, 66.
35 A. Bétard and R. A. Fischer, *Chem. Rev.*, 2012, **112**, 1055.
36 H. Gliemann and C. Wöll, *Mater. Today*, 2012, **15**, 110.
37 D. Zacher, O. Shekhah, C. Wöll and R. A. Fischer, *Chem. Soc. Rev.*, 2009, **38**, 1418.
38 O. Shekhah, H. Wang, S. Kowarik, F. Schreiber, M. Paulus, M. Tolan, C. Sternemann, F. Evers, D. Zacher, R. A. Fischer and C. Wöll, *J. Am. Chem. Soc.*, 2007, **129**, 15118.
39 O. Shekhah, H. Wang, T. Strunskus, P. Cyganik, D. Zacher, R. Fischer and C. Wöll, *Langmuir*, 2007, **23**, 7440.
40 O. Shekhah, H. Wang, D. Zacher, R. A. Fischer and C. Wöll, *Angew. Chem., Int. Ed.*, 2009, **48**, 5038.

41 V. Stavila, J. Volponi, A. M. Katzenmeyer, M. C. Dixon and M. D. Allendorf, *Chem. Sci.*, 2012, **3**, 1531.
42 O. Shekhah, *Materials*, 2010, **3**, 1302.
43 K. Otsubo, T. Haraguchi, O. Sakata, A. Fujiwara and H. Kitagawa, *J. Am. Chem. Soc.*, 2012, **134**, 9605.
44 A. S. Muench, M. S. Lohse, S. Hausdorf, G. Schreiber, D. Zacher, R. A. Fischer and F. O. R. L. Mertens, *Microporous Mesoporous Mater.*, 2012, **159**, 132.
45 A. Betard, S. Wannapaiboon and R. A. Fischer, *Chem. Commun.*, 2012, **48**, 10493.
46 R. Makiura, S. Motoyama, Y. Umemura, H. Yamanaka, O. Sakata and H. Kitagawa, *Nat. Mater.*, 2010, **9**, 565.
47 S. Motoyama, R. Makiura, O. Sakata and H. Kitagawa, *J. Am. Chem. Soc.*, 2011, **133**, 5640.
48 O. Shekhah, K. Hirai, H. Wang, H. Uehara, M. Kondo, S. Diring, D. Zacher, R. A. Fischer, O. Sakata, S. Kitagawa, S. Furukawa and C. Woell, *Dalton Trans.*, 2011, **40**, 4954.
49 H. X. Deng, C. J. Doonan, H. Furukawa, R. B. Ferreira, J. Towne, C. B. Knobler, B. Wang and O. M. Yaghi, *Science*, 2010, **327**, 846.
50 B. Liu and R. A. Fischer, *Sci. China: Chem.*, 2011, **54**, 1851.
51 S. Hermes, F. Schröder, R. Chelmowski, C. Wöll and R. A. Fischer, *J. Am. Chem. Soc.*, 2005, **127**, 13744.
52 S. Hermes, T. Witte, T. Hikov, D. Zacher, S. Bahnmuller, G. Langstein, K. Huber and R. A. Fischer, *J. Am. Chem. Soc.*, 2007, **129**, 5324.
53 C. Scherb, A. Schödel and T. Bein, *Angew. Chem., Int. Ed.*, 2008, **47**, 5777.
54 R. A. Fischer and C. Wöll, *Angew. Chem., Int. Ed.*, 2009, **48**, 6205.
55 B. Liu, M. Tu and R. A. Fischer, *Angew. Chem., Int. Ed.*, 2013, **52**, 3402.
56 B. Liu, M. Tu, D. Zacher and R. A. Fischer, *Adv. Funct. Mater.*, 2013, **23**, 3790.
57 F. M. Hinterholzinger, A. Ranft, J. M. Feckl, B. Ruehle, T. Bein and B. V. Lotsch, *J. Mater. Chem.*, 2012, **22**, 10356.
58 M. Eddaoudi, J. Kim, N. Rosi, D. Vodak, J. Wachter, M. O'Keeffe and O. M. Yaghi, *Science*, 2002, **295**, 469.
59 S. Furukawa, K. Hirai, K. Nakagawa, Y. Takashima, R. Matsuda, T. Tsuruoka, M. Kondo, R. Haruki, D. Tanaka, H. Sakamoto, S. Shimomura, O. Sakata and S. Kitagawa, *Angew. Chem., Int. Ed.*, 2009, **48**, 1766.
60 K. Koh, A. G. Wong-Foy and A. J. Matzger, *Chem. Commun.*, 2009, 6162.
61 Y. Yoo and H. K. Jeong, *Cryst. Growth Des.*, 2010, **10**, 1283.
62 M. Tu, S. Wannapaiboon and R. A. Fischer, *Dalton Trans.*, 2013, **42**, 16029.
63 M. Tu and R. A. Fischer, *J. Mater. Chem. A*, 2014, **2**, 2018.
64 W. Kleist, F. Jutz, M. Maciejewski and A. Baiker, *Eur. J. Inorg. Chem.*, 2009, 3552.
65 Y.-g. Sun, J. Li, K.-l. Li, Z.-h. Xu, F. Ding, B.-y. Ren, S.-j. Wang, L.-x. You, G. Xiong and P. F. Smet, *CrystEngComm*, 2014, **16**, 1777.
66 A. J. Heeger, *Angew. Chem., Int. Ed.*, 2001, **40**, 2591.
67 V. Coropceanu, J. Cornil, D. A. da Silva Filho, Y. Olivier, R. Silbey and J.-L. Bredas, *Chem. Rev.*, 2007, **107**, 2165.
68 N. A. Minder, S. Ono, Z. Chen, A. Facchetti and A. F. Morpurgo, *Adv. Mater.*, 2012, **24**, 503.
69 H. Miyasaka, *Acc. Chem. Res.*, 2013, **46**, 248.
70 K. Itaya and I. Uchida, *Inorg. Chem.*, 1986, **25**, 389.
71 M. B. Robin, *Inorg. Chem.*, 1962, **1**, 337.
72 B. S. Brunschwig, C. Creutz and N. Sutin, *Chem. Soc. Rev.*, 2002, **31**, 168.
73 D. M. Pajerowski, T. Watanabe, T. Yamamoto and Y. Einaga, *Phys. Rev. B: Condens. Matter Mater. Phys.*, 2011, **83**, 153202.
74 M. B. Robin and P. Day, in *Advances in Inorganic Chemistry and Radiochemistry*, ed. H. J. Emeléus and A. G. Sharpe, Academic Press, 1968, vol. 10, p. 247.
75 C. H. Hendon, D. Tiana and A. Walsh, *Phys. Chem. Chem. Phys.*, 2012, **14**, 13120.
76 H. Miyasaka, N. Motokawa, S. Matsunaga, M. Yamashita, K. Sugimoto, T. Mori, N. Toyota and K. R. Dunbar, *J. Am. Chem. Soc.*, 2010, **132**, 1532.
77 Z. Zhang, H. Zhao, H. Kojima, T. Mori and K. R. Dunbar, *Chem. – Eur. J.*, 2013, **19**, 3348.
78 J. B. Torrance, *Acc. Chem. Res.*, 1979, **12**, 79.
79 R. A. Heintz, H. H. Zhao, O. Y. Xiang, G. Grandinetti, J. Cowen and K. R. Dunbar, *Inorg. Chem.*, 1999, **38**, 144.
80 Y. Kobayashi, B. Jacobs, M. D. Allendorf and J. R. Long, *Chem. Mater.*, 2010, **22**, 4120.
81 T. C. Narayan, T. Miyakai, S. Seki and M. Dinca, *J. Am. Chem. Soc.*, 2012, **134**, 12932.
82 S. Wan, J. Guo, J. Kim, H. Ihee and D. Jiang, *Angew. Chem.*, 2008, **120**, 8958.
83 S. Wan, J. Guo, J. Kim, H. Ihee and D. Jiang, *Angew. Chem.*, 2009, **121**, 5547.
84 L. Sun, T. Miyakai, S. Seki and M. Dinca, *J. Am. Chem. Soc.*, 2013, **135**, 8185.
85 A. Dragasser, O. Shekhah, O. Zybaylo, C. Shen, M. Buck, C. Wöll and D. Schlettwein, *Chem. Commun.*, 2012, **48**, 663.
86 M. D. McGehee, *MRS Bull.*, 2009, **34**, 95.
87 M. D. Perez, C. Borek, S. R. Forrest and M. E. Thompson, *J. Am. Chem. Soc.*, 2009, **131**, 9281.
88 A. Coskun, J. M. Spruell, G. Barin, W. R. Dichtel, A. H. Flood, Y. Y. Botros and J. F. Stoddart, *Chem. Soc. Rev.*, 2012, **41**, 4827.
89 H. Song, M. A. Reed and T. Lee, *Adv. Mater.*, 2011, **23**, 1583.
90 C. A. Bauer, T. V. Timofeeva, T. B. Settersten, B. D. Patterson, V. H. Liu, B. A. Simmons and M. D. Allendorf, *J. Am. Chem. Soc.*, 2007, **129**, 7136.
91 J. J. Perry, P. L. Feng, S. T. Meek, K. Leong, F. P. Doty and M. D. Allendorf, *J. Mater. Chem.*, 2012, **22**, 10235.
92 B. Civalleri, F. Napoli, Y. Noel, C. Roetti and R. Dovesi, *CrystEngComm*, 2006, **8**, 364.
93 L. M. Yang, P. Vajeeston, P. Ravindran, H. Fjellvag and M. Tilset, *Inorg. Chem.*, 2010, **49**, 10283.
94 M. Fuentes-Cabrera, D. M. Nicholson, B. G. Sumpter and M. Widom, *J. Chem. Phys.*, 2005, **123**, 124713.
95 A. Kuc, A. Enyashin and G. Seifert, *J. Phys. Chem. B*, 2007, **111**, 8179.
96 M. E. Foster, J. D. Azoulay, B. M. Wong and M. D. Allendorf, *Chem. Sci.*, 2014, **5**, 2081.

97 H. C. Streit, M. Adlung, O. Shekhah, X. Stammer, H. K. Arslan, O. Zybaylo, T. Ladnorg, H. Gliemann, M. Franzreb, C. Wöll and C. Wickleder, *ChemPhysChem*, 2012, **13**, 2699.
98 D. P. Yan, G. O. Lloyd, A. Delori, W. Jones and X. Duan, *ChemPlusChem*, 2012, **77**, 1112.
99 Y. Takashima, S. Furukawa and S. Kitagawa, *CrystEngComm*, 2011, **13**, 3360.
100 K. Leong, M. E. Foster, B. M. Wong, E. D. Spoerke, D. V. Gough, J. C. Deaton and M. D. Allendorf, *J. Mater. Chem. A*, 2014, **2**, 3389.
101 M. Muller, X. N. Zhang, Y. M. Wang and R. A. Fischer, *Chem. Commun.*, 2009, 119.
102 G. Lu, S. Z. Li, Z. Guo, O. K. Farha, B. G. Hauser, X. Y. Qi, Y. Wang, X. Wang, S. Y. Han, X. G. Liu, J. S. DuChene, H. Zhang, Q. C. Zhang, X. D. Chen, J. Ma, S. C. J. Loo, W. D. Wei, Y. H. Yang, J. T. Hupp and F. W. Huo, *Nat. Chem.*, 2012, **4**, 310.
103 S. Y. Jin, H. J. Son, O. K. Farha, G. P. Wiederrecht and J. T. Hupp, *J. Am. Chem. Soc.*, 2013, **135**, 955.
104 D. Buso, J. Jasieniak, M. D. H. Lay, P. Schiavuta, P. Scopece, J. Laird, H. Amenitsch, A. J. Hill and P. Falcaro, *Small*, 2012, **8**, 80.
105 H. Yersin, A. F. Rausch, R. Czerwieniec, T. Hofbeck and T. Fischer, *Coord. Chem. Rev.*, 2011, **255**, 2622.
106 C. A. Kent, D. M. Liu, L. Q. Ma, J. M. Papanikolas, T. J. Meyer and W. B. Lin, *J. Am. Chem. Soc.*, 2011, **133**, 12940.
107 C. Wang and W. B. Lin, *J. Am. Chem. Soc.*, 2011, **133**, 4232.
108 J. X. Lin, X. Q. Hu, P. Zhang, A. Van Rynbach, D. N. Beratan, C. A. Kent, B. P. Mehl, J. M. Papanikolas, T. J. Meyer, W. B. Lin, S. S. Skourtis and M. Constantinou, *J. Phys. Chem. C*, 2013, **117**, 22250.
109 C. Y. Lee, O. K. Farha, B. J. Hong, A. A. Sarjeant, S. T. Nguyen and J. T. Hupp, *J. Am. Chem. Soc.*, 2011, **133**, 15858.
110 H. J. Son, S. Y. Jin, S. Patwardhan, S. J. Wezenberg, N. C. Jeong, M. So, C. E. Wilmer, A. A. Sarjeant, G. C. Schatz, R. Q. Snurr, O. K. Farha, G. P. Wiederrecht and J. T. Hupp, *J. Am. Chem. Soc.*, 2013, **135**, 862.
111 P. L. Feng, J. J. Perry, S. Nikodemski, B. W. Jacobs, S. T. Meek and M. D. Allendorf, *J. Am. Chem. Soc.*, 2010, **132**, 15487.
112 M. Alvaro, E. Carbonell, B. Ferrer, F. Xamena and H. Garcia, *Chem. – Eur. J.*, 2007, **13**, 5106.
113 H. A. Lopez, A. Dhakshinamoorthy, B. Ferrer, P. Atienzar, M. Alvaro and H. Garcia, *J. Phys. Chem. C*, 2011, **115**, 22200.
114 Y. F. Li, A. Y. Pang, C. J. Wang and M. D. Wei, *J. Mater. Chem.*, 2011, **21**, 17259.
115 J. Gascon, M. D. Hernandez-Alonso, A. R. Almeida, G. P. M. van Klink, F. Kapteijn and G. Mul, *ChemSusChem*, 2008, **1**, 981.
116 M. A. Nasalevich, M. G. Goesten, T. J. Savenije, F. Kapteijn and J. Gascon, *Chem. Commun.*, 2013, **49**, 10575.
117 T. Tachikawa, J. R. Choi, M. Fujitsuka and T. Majima, *J. Phys. Chem. C*, 2008, **112**, 14090.
118 C. Wang, Z. G. Xie, K. E. deKrafft and W. L. Lin, *J. Am. Chem. Soc.*, 2011, **133**, 13445.
119 C. Wang, K. E. deKrafft and W. B. Lin, *J. Am. Chem. Soc.*, 2012, **134**, 7211.
120 S. Hermes, M.-K. Schroter, R. Schmid, L. Khodeir, M. Muhler, A. Tissler, R. W. Fischer and R. A. Fischer, *Angew. Chem., Int. Ed.*, 2005, **44**, 6237.
121 M. D. Allendorf, R. J. T. Houk, L. Andruszkiewicz, A. A. Talin, J. Pikarsky, A. Choudhury, K. A. Gall and P. J. Hesketh, *J. Am. Chem. Soc.*, 2008, **130**, 14404.
122 I. Ellern, A. Venkatasubramanian, J.-H. Lee, P. Hesketh, V. Stavila, A. Robinson and M. Allendorf, *Micro Nano Lett.*, 2013, **8**, 766.
123 A. L. Robinson, V. Stavila, T. R. Zeitler, M. I. White, S. M. Thornberg, J. A. Greathouse and M. D. Allendorf, *Anal. Chem.*, 2012, **84**, 7043.
124 A. Venkatasubramanian, J.-H. Lee, V. Stavila, A. Robinson, M. D. Allendorf and P. J. Hesketh, *Sens. Actuators, B*, 2012, **168**, 256.
125 Q. Tang, S. Liu, Y. Liu, J. Miao, S. Li, L. Zhang, Z. Shi and Z. Zheng, *Inorg. Chem.*, 2013, **52**, 2799.
126 Y. Takashima, V. M. Martinez, S. Furukawa, M. Kondo, S. Shimomura, H. Uehara, M. Nakahama, K. Sugimoto and S. Kitagawa, *Nat. Commun.*, 2011, **2**, 168.
127 Y. Li, S. Zhang and D. Song, *Angew. Chem., Int. Ed.*, 2013, **52**, 710.
128 C. M. Doherty, G. Grenci, R. Ricco, J. I. Mardel, J. Reboul, S. Furukawa, S. Kitagawa, A. J. Hill and P. Falcaro, *Adv. Mater.*, 2013, **25**, 4701.
129 B. Liu, *J. Mater. Chem.*, 2012, **22**, 10094.